bioRxiv preprint doi: https://doi.org/10.1101/2020.12.20.423707; this version posted March 17, 2021. The copyright holder for this preprint (which was not certified by peer review) is the author/funder, who has granted bioRxiv a license to display the preprint in perpetuity. It is made available under aCC-BY-NC-ND 4.0 International license.

The assisting role of Polη in transcription facilitates formation of damage-induced cohesion

Pei-Shang Wu[1], Donald P. Cameron[1 ¶], Jan Grosser[1¶], Laura Baranello[1] and Lena Ström[1*]

[1] Karolinska Institutet, Department of Cell and Molecular Biology, SE-171 77 Stockholm, Sweden

¶ These authors contributed equally to this work

* Corresponding author

Email: lena.strom@ki.se

Short title: Transcription facilitates damage-induced cohesion

bioRxiv preprint doi: https://doi.org/10.1101/2020.12.20.423707; this version posted March 17, 2021. The copyright holder for this preprint (which was not certified by peer review) is the author/funder, who has granted bioRxiv a license to display the preprint in perpetuity. It is made available under aCC-BY-NC-ND 4.0 International license.

Abstract

The structural maintenance of chromosome (SMC) complex cohesin mediates sister chromatid cohesion established during replication, and damage-induced cohesion formed in response to DSBs post-replication. The translesion synthesis polymerase Polη is required for damage-induced cohesion through a hitherto unknown mechanism. Since Polη is functionally associated with transcription, and transcription triggers *de novo* cohesion in *Schizosaccharomyces pombe*, we hypothesized that transcription facilitates damage-induced cohesion in *Saccharomyces cerevisiae*. Here, we show dysregulated transcriptional profiles in Polη-depleted cells (*rad30Δ*), where genes involved in chromatin assembly and positive transcription regulation were downregulated. In addition, chromatin association of RNA polymerase II was reduced at promoters and coding regions in *rad30Δ* compared to WT cells, while occupancy of the H2A.Z variant (Htz1) at promoters was increased in *rad30Δ* cells. Perturbing histone exchange at promoters inactivated damage-induced cohesion, similarly to deletion of the *RAD30* gene. Conversely, altering regulation of transcription elongation suppressed the deficient damage-induced cohesion in *rad30Δ* cells. These results indicate that Polη has an assisting role during the transcriptional process, which consecutively facilitates formation of damage-induced cohesion. This further suggests a potential linkage between regulation of transcription and formation of damage-induced cohesion after replication.

bioRxiv preprint doi: https://doi.org/10.1101/2020.12.20.423707; this version posted March 17, 2021. The copyright holder for this preprint (which was not certified by peer review) is the author/funder, who has granted bioRxiv a license to display the preprint in perpetuity. It is made available under aCC-BY-NC-ND 4.0 International license.

Author Summary

The cohesin complex dynamically associates with chromosomes and holds sister chromatids together through cohesion established during replication. This ensures faithful chromosome segregation at anaphase. In budding yeast, DNA double strand breaks trigger sister chromatid cohesion even after replication. This so-called damage-induced cohesion is formed both close to the breaks, and genome-wide on undamaged chromosomes. The translesion synthesis polymerase eta (Polη) is specifically required for genome wide damage-induced cohesion. Although Polη is well characterized for its function in bypassing ultraviolet-induced DNA lesions, its mechanistic role in damage-induced cohesion is unclear. Here, we show that transcriptional regulation is perturbed in the absence of Polη. We propose that Polη could aid in chromatin association of RNA polymerase II through phosphorylation of the Polη-S14 residue, a non-canonical role of Polη which further facilitates formation of damage-induced cohesion genome wide. In addition, we observe the need of replication-independent nucleosome assembly/histone exchange for formation of damage-induced cohesion. This together provides new insight into formation of damage-induced cohesion after replication, which will be interesting to further explore.

bioRxiv preprint doi: https://doi.org/10.1101/2020.12.20.423707; this version posted March 17, 2021. The copyright holder for this preprint (which was not certified by peer review) is the author/funder, who has granted bioRxiv a license to display the preprint in perpetuity. It is made available under aCC-BY-NC-ND 4.0 International license.

Introduction

Dynamic disassembly and reassembly of nucleosomes — the building blocks of chromatin — facilitates processes such as replication and transcription. During the course of chromatin assembly, the canonical histones are exchanged with histone variants or post-translationally modified histones. This affects the physical and chemical properties of nucleosomes, as well as chromatin accessibility. Replication-independent nucleosome assembly, or so-called histone exchange, aids and regulates RNA polymerase II (RNAPII) passage through the nucleosomes during transcription initiation and elongation [1]. This is accomplished through histone chaperones, in concert with histone modifying enzymes and chromatin remodelers [2].

Transcription is not only the instrument for gene expression, but is also connected to cohesin localization on chromosomes. Cohesin is one of the structural maintenance of chromosomes (SMC) protein complexes, with the core formed by Smc1, Smc3 and the kleisin Scc1. Cohesin dynamically associates with chromosomes at intergenic regions of convergent genes, possibly as a result of active transcription [3, 4]. Cohesin and its chromatin loader Scc2 have been implicated in gene regulation [5-7] and also in spatial organization of chromosomes into topologically associated domains (TADs) through DNA loop extrusion [8-12].

In addition to the roles described above, the canonical role of cohesin is to mediate sister chromatid cohesion. Cohesin is recruited to chromatin by the cohesin loading complex Scc2-Scc4 from late G_1 phase in *S. cerevisiae* [13], and continuously through the cell cycle [14, 15]. During S-phase, cohesin becomes cohesive through acetylation of Smc3 by the acetyltransferase Eco1 [16-18]. The

bioRxiv preprint doi: https://doi.org/10.1101/2020.12.20.423707; this version posted March 17, 2021. The copyright holder for this preprint (which was not certified by peer review) is the author/funder, who has granted bioRxiv a license to display the preprint in perpetuity. It is made available under aCC-BY-NC-ND 4.0 International license.

established sister chromatid cohesion is then maintained until anaphase [19], ensuring faithful chromosome segregation.

At the end of S phase, Eco1 is targeted for degradation. However, inducing a single site-specific double strand break post-replication (G_2/M) is sufficient to stabilize Eco1 [20, 21]. Presence of active Eco1 then allows generation of damage-induced cohesion in G_2/M, which is established close to the break, and also genome wide on undamaged chromosomes [22-24]. We previously showed that Polymerase eta (Polη), one of the three translesion synthesis (TLS) polymerases in *S. cerevisiae*, is specifically required for genome wide damage-induced cohesion [25].

Polη (encoded by the *RAD30* gene) is well characterized for bypassing bulky lesions induced by ultraviolet irradiation [26], yet emerging evidence suggest that Polη also exhibits TLS-independent functions [27]. Polη is the only TLS polymerase required for damage-induced cohesion [25], independently of its polymerase activity, but dependent on Polη-S14 phosphorylation; potentially mediated by the cyclin dependent kinase, Cdc28 [28]. However, the underlying role of Polη in damage-induced cohesion remains unclear. Thus, absence of Polη does not affect break-proximal damage-induced cohesion or DSB repair. Lack of Polη also does not perturb Eco1 stabilization, cohesin chromatin association or Smc3 acetylation after induction of DSBs in G_2/M [25].

Based on the following two observations, we hypothesized that active transcription facilitates damage-induced cohesion genome wide. First, Polη is enriched at actively transcribed regions, and required for expression of several active genes in *S. cerevisiae* [29]. Second, activated transcription leads to establishment of local *de novo* cohesion in *S. pombe* [30]. Here, we present data pointing at a role for

bioRxiv preprint doi: https://doi.org/10.1101/2020.12.20.423707; this version posted March 17, 2021. The copyright holder for this preprint (which was not certified by peer review) is the author/funder, who has granted bioRxiv a license to display the preprint in perpetuity. It is made available under aCC-BY-NC-ND 4.0 International license.

Polη and Polη-S14 phosphorylation in facilitating chromatin association of RNAPII. In addition, the transcriptional program in the Polη null mutant (*rad30Δ*) is altered both before and after DSB induction, with expression of genes involved in chromatin assembly and positive transcription regulation being downregulated compared to WT cells. Perturbing histone exchange at promoter regions by a *HIR1* or *HTZ1* deletion negatively affects damage-induced cohesion formation, in a similar fashion as in *rad30Δ* cells. Deletion of the transcription elongation regulator *SET2* however, suppresses the lack of damage-induced cohesion in the *rad30Δ* mutant. Taken together, our results suggest that Polη is required for damage-induced cohesion through its assisting role in transcription, and support the hypothesis that regulated transcription facilitates formation of damage-induced cohesion.

Results

A potential role for Polη in facilitating chromatin association of RNAPII

To test if active transcription is correlated with generation of damage-induced cohesion, we initially assessed sensitivity of the damage-induced cohesion deficient *rad30Δ* and *Polη-S14A* cells to transcription elongation inhibitors. Viability of both mutants decreased when exposed to actinomycin D (Fig 1A). In addition, consistent with a previous report [29], *rad30Δ* cells were sensitive to mycophenolic acid (MPA). This was also true for the *Polη-S14A* point mutant (Fig 1A). Sensitivity of both mutants to MPA was reversed by supplementing guanine in the media (Fig 1A), verifying that it was due to depletion of the guanylic nucleotide pool [31].

bioRxiv preprint doi: https://doi.org/10.1101/2020.12.20.423707; this version posted March 17, 2021. The copyright holder for this preprint (which was not certified by peer review) is the author/funder, who has granted bioRxiv a license to display the preprint in perpetuity. It is made available under aCC-BY-NC-ND 4.0 International license.

Sensitivity to elongation inhibitors might be due to reduced transcriptional capacity. We therefore monitored chromatin association of Rpb1, the largest subunit of RNAPII, in these mutants. Binding of Rpb1 at promoters and coding regions of selected active genes was reduced in both *rad30Δ* and *Polη-S14A* mutants compared to WT cells (Fig 1B). The reduced chromatin association was accompanied by an increased level of total Rpb1 (Figs 1C and S1A). Furthermore, Rpb1 stability in the *rad30Δ* and *Polη-S14A* mutants was not affected, regardless of DSB induction (Figs 1C and 1D, S1A and S1B). Here and throughout the study the DSBs were induced at the *MAT* locus on chromosome III (P_{GAL}-*HO*) for one-hour, unless otherwise stated. These results together suggest that Polη facilitates chromatin association of RNAPII for proper transcription initiation and elongation, independent of DNA damage, likely through phosphorylation of Polη-S14.

Transcription is perturbed in *rad30Δ* mutants

To further pinpoint a potential connection between transcription and formation of damage-induced cohesion, we focused on the *rad30Δ* mutant for the following investigations. To begin with, we analyzed gene expression of G_2/M arrested WT and *rad30Δ* cells, before and after one-hour break induction, by RNA-sequencing analysis (RNA-seq). Prior to RNA-seq, G_2/M arrest and break induction were confirmed (S2A and S2B Fig). Principal component analysis (PCA) showed that the individual data sets were distributed as distinct clusters (S2C Fig). Differences in gene expression patterns between WT and *rad30Δ* cells were readily observed before break induction, with 395 genes upregulated and 439 genes downregulated in the G_2/M arrested *rad30Δ* mutant (Fig 2A). In response to DSB induction, the WT

bioRxiv preprint doi: https://doi.org/10.1101/2020.12.20.423707; this version posted March 17, 2021. The copyright holder for this preprint (which was not certified by peer review) is the author/funder, who has granted bioRxiv a license to display the preprint in perpetuity. It is made available under aCC-BY-NC-ND 4.0 International license.

cells showed 473 genes up- and 519 genes down-regulated (Fig 2B), whereas there were 360 genes up- and 230 genes down-regulated in the *rad30Δ* mutant (Fig 2C, S1 Data). While the differentially expressed genes in WT and *rad30Δ* cells after break induction significantly overlapped (S2D Fig) and trended in the same direction, the up- and down-regulation after DSB was of greater magnitude in the WT cells (Fig 2D and 2E). This implied that the response to break induction in the *rad30Δ* cells is similar, but relatively attenuated in comparison to the response in WT cells. Furthermore, we noted that short genes were preferentially upregulated compared to long genes in WT cells after DSB induction (Fig 2F), similar to the reported gene length dependent changes of expression after UV exposure [32, 33]. In contrast, differential expression after DSBs is independent of gene length in the *rad30Δ* mutant (Fig 2F). From these results we conclude that *RAD30* deletion leads to transcription deregulation, both in unperturbed G_2/M phase and in response to break induction.

Downregulated genes in G_2/M arrested *rad30⊿* cells are enriched for closed- and TATA-containing promoters

To gain additional insight into the role of Polη during transcription, we used published datasets to analyze if the deregulated genes in *rad30Δ* cells were associated with specific types of promoters, in a similar manner as reported [34]. These datasets classify genes according to type of promoter: (i) open/closed promoters, either with or without a nucleosome free region [35], (ii) promoters with fragile/stable nucleosome, defined by sensitivity of the -1 nucleosome to MNase digestion [36], and (iii) the canonical TATA-containing or TFIID dominated promoters

bioRxiv preprint doi: https://doi.org/10.1101/2020.12.20.423707; this version posted March 17, 2021. The copyright holder for this preprint (which was not certified by peer review) is the author/funder, who has granted bioRxiv a license to display the preprint in perpetuity. It is made available under aCC-BY-NC-ND 4.0 International license.

[37, 38]. Notably, a significant number of downregulated genes in G_2/M arrested *rad30Δ* cells were classified under the group of closed promoters (Table 1). In addition, the up- and down-regulated genes in G_2/M arrested *rad30Δ* cells were dominated by TATA-containing promoters (obs/exp>1). These imply that Polη more frequently associates with promoters in closed configuration and TATA-containing promoters, primed for transcriptional activation in G_2/M phase.

Table 1. Association of differentially expressed genes with promoter type in G_2/M arrested *rad30Δ* cells

rad30Δ G2 vs. WT G2	**upregulated (395)**			**downregulated (439)**		
	overlap	obs/exp	*p* values	overlap	obs/exp	*p* values
closed promoter (1596)	118	1.1	0.046	146	**1.3**	3.309e-04 *
open promoter (3504)	228	1.0	0.459	237	0.9	0.077
FN promoter (1953)[a]	139	1.1	0.086	156	1.1	0.054
SN promoter (3066)[b]	206	1.0	0.223	245	1.1	0.008
TATA-containing (1090)	96	**1.4**	6.726e-04 *	132	**1.7**	5.069e-11 *
TFIID-dominated (5130)	299	0.9	7.636e-06 *	326	0.9	4.377e-08 *

Number of genes in each group is indicated in parentheses. The numbers in bold indicate that the overlap is higher than expected, observation/expectation (obs/exp)>1. Asterisks indicate significant overlap (p<0.001), evaluated as described in materials and methods. [a]FN: fragile nucleosome, [b]SN: stable nucleosome.

Increased cohesin binding around TSS in *rad30Δ* cells

Since active transcription results in cohesin localization at the ends of convergent genes [3, 39], we considered that the observed transcriptional deregulation in the *rad30Δ* mutant could affect cohesin dynamics on chromosomes. To address this possibility, we re-analyzed our previously published Scc1 ChIP-sequencing dataset (GSE42655), from which it was concluded that cohesin binding was similar with and without break induction in the WT cells, except at the break site.

bioRxiv preprint doi: https://doi.org/10.1101/2020.12.20.423707; this version posted March 17, 2021. The copyright holder for this preprint (which was not certified by peer review) is the author/funder, who has granted bioRxiv a license to display the preprint in perpetuity. It is made available under aCC-BY-NC-ND 4.0 International license.

In addition, absence of Polη did not result in apparent differences in overall cohesin binding [25]. The upregulation of short genes in WT cells after DSB induction (Fig 2F) also appeared to be independent of cohesin binding (S2E Fig). Thus, transcription responses in general do not seem to directly correlate with cohesin distribution in G_2/M phase. However, when focusing on cohesin binding at transcription start site (TSS) and transcription end site (TES), accumulation of cohesin around TSS was increased in *rad30Δ* compared to WT cells (Fig 3A and 3B). Notably, this increased accumulation was not found around TES (Fig 3C and 3D), and was independent of DSB induction (Fig 3A-D). This could reflect that cohesin associated around TSS becomes less dynamic when transcription is dysregulated, regardless of DSB induction.

Genes involved in chromatin assembly and positive transcription regulation pathways are downregulated in the absence of Polη

To gain mechanistic insight into the diverse transcriptional responses detected in WT and *rad30Δ* cells, differential gene expression between WT and *rad30Δ* cells (before and after DSBs) were analyzed by Gene Set Enrichment Analysis (GSEA), followed by generation of enriched pathway maps with Cytoscape as shown in Fig 4. The gene sets under each annotated group are listed in S2 and S3 Data. During G_2/M arrest, genes that belong to biological pathways such as chromatin assembly and positive transcription regulation were downregulated in *rad30Δ* compared to WT cells (Fig 4A). Consistent with downregulation of the genes involved in chromatin assembly pathway, we observed that the nucleosome occupancy of *rad30Δ* cells was moderately increased compared to WT cells (S3A Fig). When comparing gene

bioRxiv preprint doi: https://doi.org/10.1101/2020.12.20.423707; this version posted March 17, 2021. The copyright holder for this preprint (which was not certified by peer review) is the author/funder, who has granted bioRxiv a license to display the preprint in perpetuity. It is made available under aCC-BY-NC-ND 4.0 International license.

expression after break induction, the pathways illustrated in Fig 4B were clearly differentially regulated between WT and *rad30Δ* cells. WT cells tended to downregulate essential cell homeostatis pathways, such as ribosome biogenesis and various metabolism pathways, relative to the *rad30Δ* mutant. This further indicates deregulation of gene expression in the *rad30Δ* mutant. Despite that some genes belonging to the cellular response to DNA damage stimulus pathway (GO: 6974) were upregulated in WT cells after DSB induction, this pathway was overall not significantly enriched. In addition, activation of the DNA damage checkpoint, as indicated by phosphorylation of Rad53, was only observed during the recovery period after DSB induction in WT and *rad30Δ* cells (S3B and S3C Fig), with no difference in cell cycle progression between populations (S3D Fig). These results indicate that the lack of damage-induced cohesion in *rad30Δ* cells is not due to a possible difference in activation of the DNA damage checkpoint. Furthermore, in response to DSBs, expression of the acetyltransferase *ECO1* was not enhanced in either WT or *rad30Δ* cells (S3E Fig). Based on this, it is plausible to test the potential connection between transcription and damage-induced cohesion, by focusing on two of the upregulated gene sets in the WT cells before DSB induction — chromatin assembly and positive transcription regulation.

Deleting *HIR1* leads to partially deficient damage-induced cohesion

To test if active transcription facilitates formation of damage-induced cohesion genome-wide, we treated cells briefly with the transcription inhibitor thiolutin to block transcription before γ-irradiation. However, we observed that the thiolutin treatment itself triggered an early DNA damage response (S4A Fig). Since the γ-H2AX signal

bioRxiv preprint doi: https://doi.org/10.1101/2020.12.20.423707; this version posted March 17, 2021. The copyright holder for this preprint (which was not certified by peer review) is the author/funder, who has granted bioRxiv a license to display the preprint in perpetuity. It is made available under aCC-BY-NC-ND 4.0 International license.

was comparable to that in irradiated cells without thiolutin (S4A Fig), we concluded that using thiolutin in our damage-induced cohesion assay is not applicable. Therefore, to test if transcriptional activity is related to generation of damage-induced cohesion, we set out to utilize a genetic approach by testing mutants which would either mimic or reverse the transcriptional deregulation in *rad30Δ* cells.

To this end, from the perspective of chromatin assembly, we investigated whether Hir1 (a component of the HIR complex) is required for damage-induced cohesion. The HIR complex and the histone chaperone Asf1 mediate histone H3 exchange with post-translationally modified H3, independently of replication [40, 41]. The exchange mainly takes place at promoters and correlates with active transcription. However, basal H3 exchange also occurs to poise inactive promoters for optimal transcription [42, 43]. To monitor damage-induced cohesion, DSBs and ectopic P_{GAL}-*SMC1-MYC* expression were induced by addition of galactose to G_2/M arrested cells. Due to the *smc1-259 ts* background, cohesion established during replication was inactivated by raising the temperature. Damage-induced cohesion generated with the ectopic Smc1-Myc was examined with an integrated TetO/TetR-GFP array on Chr. V (illustrated in S4B Fig). G_2/M arrest, break induction and protein expression of the ectopic Smc1-Myc were confirmed for all experiments, with examples shown in S4C-S4E Fig. Interestingly, formation of damage-induced cohesion was partially deficient in the *hir1Δ* mutant, while the *hir1Δrad30Δ* double resembled the *rad30Δ* single mutant, although with slower sister separation (Fig 5A). This indicated that Hir1 and Polη are both required for efficient damage-induced cohesion; possibly acting in the same pathway.

With the *hir1Δ* mutant we aimed at testing if the role of the HIR complex in chromatin assembly affected formation of damage-induced cohesion. However, the

bioRxiv preprint doi: https://doi.org/10.1101/2020.12.20.423707; this version posted March 17, 2021. The copyright holder for this preprint (which was not certified by peer review) is the author/funder, who has granted bioRxiv a license to display the preprint in perpetuity. It is made available under aCC-BY-NC-ND 4.0 International license.

observed deficiency of the *hir1Δ* cells might be due to de-repression of histone genes, as the HIR complex also negatively regulates histone genes expression [44, 45]. If so, reducing the histone gene dosage should be beneficial for the *rad30Δ* mutant in generation of damage-induced cohesion. Yet, deletion of any H3-H4 coding gene pair (*HHT1-HHF1* and *HHT2-HHF2*) did not affect formation of damage-induced cohesion in *rad30Δ* cells (Fig 5B and 5C). This indicates that the partial deficiency of the *hir1Δ* mutant is not due to altered histone gene dosage, and points to a need for histone exchange during transcription for formation of damage-induced cohesion.

Perturbing histone exchange at promoters negatively affects formation of damage-induced cohesion

To further investigate the effect of pertubing histone exchange on formation of damage-induced cohesion, we tested requirement of the H2A variant Htz1 (H2A.Z) in this process. Htz1 is preferentially incorporated at basal/repressed promoters. Susceptibility of Htz1 to loss from the incorporated nucleosome promotes its exchange for H2A. This facilitates transcriptional activation [46, 47], and relieves the +1 nucleosome barrier to RNAPII [48, 49]. Since the *htz1Δ* mutant does not respond to P_{GAL}-*HO* induction [50], γ-irradiation was utilized as source of DSB induction (see materials and methods). Similar to the *hir1Δ* mutant (S5A and S5B Fig), the *htz1Δ* mutant showed impaired damage-induced cohesion (Fig 6A). We noted that in contrast to a previous report [51], we did not observe a cohesion maintenance defect due to *HTZ1* deletion (S5C Fig).

Since Htz1 is required for formation of damage-induced cohesion, we investigated if there was a difference between WT and *rad30Δ* cells in Htz1

bioRxiv preprint doi: https://doi.org/10.1101/2020.12.20.423707; this version posted March 17, 2021. The copyright holder for this preprint (which was not certified by peer review) is the author/funder, who has granted bioRxiv a license to display the preprint in perpetuity. It is made available under aCC-BY-NC-ND 4.0 International license.

occupancy at promoters. For this, we focused on the active genes analyzed for Rpb1 binding in Fig 1B and a few genes around the *URA3* on Chr. V, where we monitored damage-induced cohesion. We further selected genes with TATA-less promoters for analyses because Htz1 is relatively enriched at these promoters [46, 47]. Interestingly, Htz1 occupancy at some of the selected promoters was significantly increased in *rad30Δ* compared to WT cells, particularly after DSB induction in G_2/M (Fig 6B and 6C). This indicates that the Htz1/H2A exchange at certain promoters was reduced in the absence of Polη, especially in response to DSB. These results were in line with *hir1Δ* and *htz1Δ* cells being deficient in damage-induced cohesion (Figs 5A, 6A and S5B), and suggest that perturbing histone exchange at promoters negatively affects formation of damage-induced cohesion.

The assisting role of Polη in transcription is needed for generation of damage-induced cohesion

In addition to the *hir1Δ* and *htz1Δ* mutants, we utilized a *set2Δ* mutant to test if transcriptional regulation is correlated with generation of damage-induced cohesion. Set2 mediates co-transcriptional H3K36 methylation (H3K36me2/3). This promotes restoration of chromatin to the pretranscribed hypoacetylation state and represses histone exchange at coding regions during transcription elongation [52-54]. Presence of Set2 at promoters also suppresses transcription initiation of certain basal repressed genes [55-57]. Interestingly, a *set2Δ* mutant suppressed sensitivity of certain transcriptional elongation factor mutants to 6-azauracil [57], a mechanistic analog of MPA [58, 59]. As we showed that *rad30Δ* cells are sensitive to transcription elongation inhibitors (Fig 1A), we tested if deletion of *SET2* would

bioRxiv preprint doi: https://doi.org/10.1101/2020.12.20.423707; this version posted March 17, 2021. The copyright holder for this preprint (which was not certified by peer review) is the author/funder, who has granted bioRxiv a license to display the preprint in perpetuity. It is made available under aCC-BY-NC-ND 4.0 International license.

rescue *rad30Δ* cells from being sensitive to these inhibitors. The *set2Δ* mutant showed no obvious sensitivity to MPA or actinomycin D, and masked the sensitivity of *rad30Δ* cells especially to actinomycin D (Fig 7A). This suggests that Set2 could counteract Polη during transcription elongation. Through this genetic interaction, we tested if deletion of *SET2* would also suppress the deficiency of *rad30Δ* cells in damage-induced cohesion. The *set2Δ* mutant resembled the WT cells in formation of damage-induced cohesion. Remarkably, deletion of *SET2* suppressed the lack of damage-induced cohesion in the *rad30Δ* mutant (Fig 7B). Given that removing *SET2* caused an increased RNAPII association towards the 3'-end of actively transcribed genes [60], we monitored chromatin association of Rpb1 in the *set2Δrad30Δ* mutant. Absence of Set2 in G_2/M arrested *rad30Δ* cells to some extend compensated for the reduced Rpb1 binding in *rad30Δ* cells (Fig 7C-7E). This trend was however not observed after DSB induction (S6A-C Fig). Considering that the differentially expressed genes in WT and *rad30Δ* cells after DSB significantly overlapped (S2D Fig), the data together suggest that general transcriptional regulation during G_2/M phase influences formation of damage-induced cohesion, and indicate that Polη is required for damage-induced cohesion through facilitating transcription.

Discussion

We previously showed that Polη is specifically required for genome wide damage-induced cohesion [25] but its mechanistic role in this process was unclear. This study was initiated by the observation that Polη-deficient cells displayed altered transcriptional regulation, both in unchallenged G_2/M arrested cells and in response to DSBs. Transcription elongation deficiency was corroborated by increased

bioRxiv preprint doi: https://doi.org/10.1101/2020.12.20.423707; this version posted March 17, 2021. The copyright holder for this preprint (which was not certified by peer review) is the author/funder, who has granted bioRxiv a license to display the preprint in perpetuity. It is made available under aCC-BY-NC-ND 4.0 International license.

sensitivity of Polη-deficient cells to transcription elongation inhibitors (Fig 1A). It could be argued that the sensitivity to actinomycin D would be a consequence of DNA damage because actinomycin D also inhibits topoisomerases [61], leading to formation of DSBs. However, since the *rad30Δ* mutant is insensitive to specific topoisomerase inhibitors, such as camptothecin and etoposide [62, 63], this was less likely.

To know which pathways were affected in the absence of Polη, gene set enrichment analysis was performed after RNA-seq. We found that mitochondrial related pathways were enhanced in *rad30⊿* cells, in contrast to downregulation of genes belonging to the chromatin assembly pathway (Fig 4A and 4B, S2 and S3 Data). This is an interesting observation since genes involved in the tricarboxylic acid cycle and oxidative phosphorylation pathways, which are related to mitochondria, were similarly upregulated in mutants with defective chromatin assembly [64].

To test the idea that the lack of damage-induced cohesion in *rad30Δ* cells would be due to transcriptional dysregulation, we began by testing the requirement of HIR/Asf1 mediated histone exchange for damage-induced cohesion, from the perspective of chromatin assembly. By deleting the *HIR1* gene, which is sufficient to disrupt the HIR/Asf1 interaction [41], we found that the *hir1Δ* mutant is partially deficient in damage-induced cohesion (Figs 5A and S5B). The role of the HIR complex in damage-induced cohesion might appear difficult to pinpoint since it is involved in multiple processes. We thus addressed the possible effect of HIR-dependent repression of histone genes [44] on formation of damage-induced cohesion. This possibility was however excluded because no effect of deleting H3-H4 gene pairs (Fig 5B and 5C) was observed in *rad30Δ* cells. The HIR complex has also been implicated in formation of a functional kinetochore [65] and heterochromatic

bioRxiv preprint doi: https://doi.org/10.1101/2020.12.20.423707; this version posted March 17, 2021. The copyright holder for this preprint (which was not certified by peer review) is the author/funder, who has granted bioRxiv a license to display the preprint in perpetuity. It is made available under aCC-BY-NC-ND 4.0 International license.

gene silencing [66]. However, the chromatin assembly complex-1 (CAF-1) is redundant with the HIR complex in these processes. Deletion of Hir1 is thereby not likely to perturb other processes than histone exchange. We therefore suggest a direct role for HIR-dependent histone exchange in damage-induced cohesion.

Functional importance of Polη in transcription was proposed to depend on its polymerase activity [29], while its role in damage-induced cohesion was not [25]. The finding that transcription facilitates formation of damage-induced cohesion could therefore be seen as conflicting with the polymerase-independent role of Polη. However, we previously showed that the putative Polη-S14 phosphorylation is required for damage-induced cohesion, but not for cell survival after UV irradiation [28], which depends on Polη polymerase activity. In addition, the *Polη-S14A* mutant exhibits similar elongation inhibitor sensitivity and altered Rpb1 behaviour as the *rad30Δ* mutant (Fig 1A-D). This together indicates that the polymerase activity is not the sole requirement for Polη in transcription.

To gain further insight into the role of Polη in transcription, we analyzed the types of promoters that Polη might associate with (Table 1). We found that the differentially expressed genes in G_2/M arrested *rad30Δ* cells, especially the downregulated genes, were relatively enriched for closed and TATA-containing promoters. The closed promoters that lack a nucleosome free region, are known to regulate stress related genes [67]. This is consistent with the downregulation of stress response (GO:0033554) in G_2/M arrested *rad30Δ* cells (S2 Data, Ungrouped). In addition, the TATA-box containing genes are highly regulated and associated with stress response [37]. Despite this information, it is still unclear in which way Polη facilitates chromatin association of Rpb1 (Fig 1), and how it affects Htz1/H2A exchange at promoters (Fig 6C). We speculate that Polη might serve as a scaffold

bioRxiv preprint doi: https://doi.org/10.1101/2020.12.20.423707; this version posted March 17, 2021. The copyright holder for this preprint (which was not certified by peer review) is the author/funder, who has granted bioRxiv a license to display the preprint in perpetuity. It is made available under aCC-BY-NC-ND 4.0 International license.

protein for Rpb1 or other transcription factors to bind on chromatin, possibly through phosphorylation of the Polη-S14 residue. Further validation of the promoters that Polη preferentially associated with might provide additional clues on potential interacting transcription factors. Nevertheless, the precise role of Polη in transcription needs to be further explored.

In addition to perturbed transcriptional regulation (Fig 2), increased cohesin binding around TSS was observed in *rad30Δ* cells, independently of DSBs (Fig 3). This indicates that transcriptional regulation might also modulate the dynamics and/or positioning of cohesin at cohesin associated regions. Since the boundaries of cohesin mediated TAD-like structures often form at promoters of active genes in yeast [68], a reciprocal interplay between transcription and formation of TAD-like structure has been suggested [69]. Although this might not be directly relevant to formation of damage-induced cohesion, it would still be interesting to investigate if TAD-like structures are altered in *rad30Δ* cells, in connection with this potential reciprocal interplay.

Through perturbing histone exchange and removing a transcription elongation regulator (depicted in S7 Fig), we show that a regulated transcriptional response connected to chromatin assembly potentially facilitates generation of damage-induced cohesion post-replication. Since establishment of sister chromatid cohesion is proposed to occur simultaneously with replication fork progression [14, 70] in concert with replication-coupled nucleosome assembly [71], we propose that replication-independent nucleosome assembly could be utilized as an alternative platform for generation of damage-induced cohesion after replication (S7 Fig, WT). Deregulated transcription in *rad30Δ* cells, which perturbs histone exchange, would in turn affect formation of damage-induced cohesion (S7 Fig, *rad30Δ*).

bioRxiv preprint doi: https://doi.org/10.1101/2020.12.20.423707; this version posted March 17, 2021. The copyright holder for this preprint (which was not certified by peer review) is the author/funder, who has granted bioRxiv a license to display the preprint in perpetuity. It is made available under aCC-BY-NC-ND 4.0 International license.

Despite the subtle defect in chromosome segregation observed in the *rad30Δ* mutant [25], the importance of genome wide damage-induced cohesion remains to be determined. It might be relevant to the increased chromosome mobility in response to DSBs, which presumably facilitates the search of sequence homology for recombination [72, 73]. Interestingly, the movement at the same time is constrained by sister chromatid cohesion [74]. Since unbroken chromosomes are known to be less mobile than broken chromosomes [72, 73], formation of genome-wide damage-induced cohesion might further limit the movements of undamaged chromosomes, to reduce the chance of unfavorable recombinations.

In summary, we show that Polη could be an auxiliary factor for transcription and that this role facilitates formation of damage-induced cohesion. Through a genetic approach, our study provides new insight into a potential linkage between histone exchange and generation of damage-induced cohesion post-replication. Futher studies would be needed to understand how Polη aids in transcription, how chromatin dynamics during transcription facilitate formation of genome wide damage-induced cohesion, and if damage-induced cohesion could restrict movements of undamaged chromosomes.

Materials and methods

Yeast strains and media

All *S. cerevisiae* yeast strains, listed in S1 Table, were W303 derivatives (*ade2-1 trp1-1 can1-100 leu2-3, 112 his3-11, 15 ura3-1 RAD5 GAL psi*$^{+}$). To create null mutants, the gene of interest was replaced with an antibiotic resistance marker

bioRxiv preprint doi: https://doi.org/10.1101/2020.12.20.423707; this version posted March 17, 2021. The copyright holder for this preprint (which was not certified by peer review) is the author/funder, who has granted bioRxiv a license to display the preprint in perpetuity. It is made available under aCC-BY-NC-ND 4.0 International license.

through lithium acetate based transformation. Some strains were crossed to obtain desired genotypes. Yeast extract peptone (YEP) supplemented with 40 µg/ml adenine was used as yeast media, unless otherwise stated.

Spot assay

Cell culturing and subsequent serial dilutions were performed as described . Each dilution was sequentially spotted on uracil drop-out (-Ura) media, containing actinomycin D, MPA, or solvent only (final 1.2% ethanol in plates). Guanine was supplemented at 0.3 mM final concentration [75]. The plates were kept at room temperature and documented on the third day. Each spot assay was done at least twice.

Protein extraction and western blotting

Whole cell extracts (WCEs) were prepared with glass bead disruption, TCA or a sodium hydroxide based method [76]. To monitor Rpb1 stability, cycloheximide (Sigma) was supplemented in media (final 100µg/ml), and the protein extracts were prepared with sodium hydroxide based method. Bolt 4-12% Bis-Tris or NuPAGE 3-8% Tris-Acetate gels (Invitrogen) were used for electrophoresis, with Bolt MOPS, Bolt MES or NuPAGE Tris-Acetate SDS running buffer (Invitrogen). Proteins were transferred to nitrocellulose membranes with the Trans-blot Turbo system (Bio-Rad) or the XCell II Blot Module (Invitrogen). Antibody information is listed in the S2 Table. Odyssey Infrared Imaging and BioRad chemiluminescence system were used for antibodies detections. Image Studio Lite software was used for quantitation of protein bands.

bioRxiv preprint doi: https://doi.org/10.1101/2020.12.20.423707; this version posted March 17, 2021. The copyright holder for this preprint (which was not certified by peer review) is the author/funder, who has granted bioRxiv a license to display the preprint in perpetuity. It is made available under aCC-BY-NC-ND 4.0 International license.

Chromatin immunoprecipitation (ChIP) qPCR

ChIP was in essence performed as described with some modifications [25]. Cells were crosslinked with final 1% formaldehyde for 20 minutes at room temperature, followed by addition of final 125 mM glycine for 5 minutes. The cells were washed three times in 1X cold TBS and mechanically lysed using a 6870 freezer/mill (SPEX, CertiPrep). WCEs were subjected to chromatin shearing by sonication (Bandelin, Sonopuls) for chromatin fragments of 3-500 bp. Anti-Rpb1 and anti-Htz1 antibodies were coupled to protein A and protein G Dynabeads (Invitrogen) respectively for immunoprecipitation at 4°C, overnight. Crosslinking of eluted IP and input samples was reversed, and DNA was purified. DNA analysis was performed by real time qPCR using SYBR Green (Applied Biosystems), according to manufacturer's guidelines on an ABI Prism 7000 sequence detection system (Applied Biosystems). The genes of interest were selected based on the RNA-seq results. Primers used are listed in S3 Table. Statistical analysis was performed with SPSS statistics software (IBM).

Total RNA extraction

For RNA-seq, G_2/M arrested cells (about 9 OD_{600}) were harvested before and after 1-hour P_{GAL}-*HO* break induction. Equal amount of samples were additionally collected at each time-point as genomic DNA (gDNA) controls. The gDNA content of each sample was determined prior to total RNA extraction. Total RNA extracts were prepared with PureLink RNA Mini Kit (Invitrogen), with some modifications of the manufacture's guidelines. Collected cell pellets were washed once with SE mix (final

bioRxiv preprint doi: https://doi.org/10.1101/2020.12.20.423707; this version posted March 17, 2021. The copyright holder for this preprint (which was not certified by peer review) is the author/funder, who has granted bioRxiv a license to display the preprint in perpetuity. It is made available under aCC-BY-NC-ND 4.0 International license.

1 M sorbitol and 50 mM EDTA), and resupended with 100 µl zymolyase lysis buffer (SE mix supplemented with final 3 mg/ml 100T zymolyase (Sunrise Science) and 2.5 µl Ribolock (Invitrogen). The suspension was incubated at 30°C for 60 minutes, followed by addition of 200 µl kit-provided RNA lysing buffer, supplemented with Ribolock. The rest of the procedure was performed according to the manufacture's guidelines. To elute total RNA from columns, the volume of RNase free water for elution was adjusted according to gDNA content of each sample. For each strain, equal volume of the total RNA extract was further purified with DNA-free Kit (Invitrogen).

RNA-sequencing and ChIP-sequencing data analyses

Total RNA samples prepared for RNA-seq (triplicates) were subsequently handled by Novogene for mRNA enrichment, library construction (250-300 bp insert cDNA library) and RNA sequencing (Illumina HiSeq X Ten, paired-end, 10 M reads). Quality controls were included for the total RNA samples and during the procedures for RNA-sequencing.

FASTQC (https://www.bioinformatics.babraham.ac.uk/projects/fastqc/) was used for quality control of the .fastq-files for both RNA- and ChIP-seq. Adapter and poor quality read trimming was performed with cutadapt [77]. The RNA-seq data was mapped with the splice-aware aligner HISAT2 [78]. The ChIP-seq data was mapped using bowtie [79] with the colorspace option enabled. Afterwards the mapped files were sorted using samtools [80]. Both sets of sequencing data were aligned to the yeast genome version SacCer3 downloaded from UCSC genome browser.

bioRxiv preprint doi: https://doi.org/10.1101/2020.12.20.423707; this version posted March 17, 2021. The copyright holder for this preprint (which was not certified by peer review) is the author/funder, who has granted bioRxiv a license to display the preprint in perpetuity. It is made available under aCC-BY-NC-ND 4.0 International license.

Duplicates in the mapped .bam-files were removed using MarkDuplicates (http://broadinstitute.github.io/picard) from the Picard toolset.

For the RNA-seq data set, the reads were counted per gene using featureCounts [81]. The count-files were imported into R and further analyzed using edgeR [82, 83] for FPKM calculations and DESeq2 [84] for differential expression analysis. Differential expression analysis yielded fold-changes alongside significance for genes, additionally DESeq2 was used to generate principal component analysis plots. Genes with a total read count below 10 across all samples as well as those producing NAs (not available) in any of the comparisons for fold-change calculation were excluded from the analysis. As all four conditions showed a similar within-group variability in the PCA plot, for all fold-change calculations all samples were run together as opposed to subsetting the samples of interest e.g. WT G2 + DSB vs. WT G2. This allowed for more accurate estimation of the dispersion parameter and in turn calculation of significance for the fold-changes. Also, the moving average of the fold-change was calculated by ordering the genes included in the DESeq2 dataset by length and then calculating the median of a window of 300 genes around these gene. No moving average was calculated for the 75 longest and shortest genes as they did not have an even number of genes on either site for moving average calculation.

For the ChIP-seq dataset, cohesin peaks were called using MACS2 [85]. The files generated were then imported into R, where they were annotated using the package ChIPpeakAnno [86] with gene lists downloaded using the biomaRt package [87]. The lists of genes overlapping or with their gene end closest to the peak middle with cohesin peaks were read into ngs.plot [88] for metagenome analysis. After analysis had been performed, the data were replotted using the internal R plotting.

bioRxiv preprint doi: https://doi.org/10.1101/2020.12.20.423707; this version posted March 17, 2021. The copyright holder for this preprint (which was not certified by peer review) is the author/funder, who has granted bioRxiv a license to display the preprint in perpetuity. It is made available under aCC-BY-NC-ND 4.0 International license.

Gene set enrichment analysis (GSEA) was performed using the Broad Institute software (http://www.broad.mit.edu/gsea) [89] using *S. cerevisiae* gene sets from the Xijin Ge lab (http://ge-lab.org/#/data) [90]. The GSEA enrichment map was created using the EnrichmentMap plugin [91] for Cytoscape [92], broadly following a published protocol [93]. Groupings were facilitated by the Cytoscape AutoAnnotate plugin [94]. In the comparison of WT vs. *rad30Δ* cells, only gene sets enriched with an adjusted *p*-value of < 0.05 were plotted. In the comparison of both WT and *rad30Δ* cells ± DSB induction, only gene sets enriched with an adjusted *p*-value of < 0.05 and a normalized enrichment score (NES) > 2 for either strain were plotted.

Statistical significance of the overlapping genes in the Venn diagrams and Table 1 were calculated using either a normal approximation or the hypergeometric probability formula. The online tool on http://nemates.org/MA/progs/overlap_stats.html was used for evaluation.

Damage-induced cohesion assay and controls

All strains used harbor the *smc1* temperature sensitive allele (*smc1-259*). The experiments with the P_{GAL}-*HO* allele for DSB induction were performed as described [28], and illustrated in S4B Fig. The assay utilizing γ-irradiation as DSB source is described in S5A Fig. Considering that the *htz1Δ* mutant is benomyl sensitive [95], the strains used in this assay contain the P_{MET}-*CDC20* and *smc1-259 ts* alleles. The strains were grown in methionine drop-out media (-Met) to log phase at 23°C. To arrest cells in G_2/M phase, expression of *CDC20* was repressed by replacing the media to YEP supplemented with Met (final 2 mM) and 0.1% glucose. Galactose (final 2%) was then added for 1.5 hours to induce expression of ectopic Smc1-Myc,

bioRxiv preprint doi: https://doi.org/10.1101/2020.12.20.423707; this version posted March 17, 2021. The copyright holder for this preprint (which was not certified by peer review) is the author/funder, who has granted bioRxiv a license to display the preprint in perpetuity. It is made available under aCC-BY-NC-ND 4.0 International license.

driven by the *GAL* promoter. The cultures were subsequently split into half and resuspended in 1X PBS. One half for γ-irradiation (250 Gy), and another half as non-irradiated control. After 1-hour recovery in YEP media supplemented with galactose and Met, the temperature was raised to 35°C and damage-induced cohesion was monitored for 90 minutes.

Proper G_2/M arrest, expression of the ectopic Smc1-Myc and DSBs induction in these assays were confirmed with FACS analysis, western blot, and pulsed-field gel electrophoresis (PFGE) respectively . Efficiency of γ-irradiation was analyzed with Southern blot after PFGE, with a probe for chromosome XVI, as described [96].

MNase digestion assay

G_2/M arrested cells were crosslinked *in vivo* with formaldehyde (final 0.5%), for 20 minutes at 23°C. To quench the reaction, glycine (final 125 mM) was added in cultures for 10 minutes. The cells were then harvested and stored at -80°C. Prior to MNase digestion, the cells were resuspended in pre-incubation solution (final 20 mM citric acid, 20 mM Na_2HPO_4, 40 mM EDTA, pH 8.0), with aliquots taken for cell-counting. The final volume of resuspension was subsequently adjusted to have 4.5 x 10^7 cells/ml. The cells were pre-treated with freshly added 2-mercaptoethanol (2-ME, final 30 mM in pre-incubation buffer) for 10 minutes at 30°C, followed by zymolyase treatment in zymolyase buffer (final 1 M sorbitol, 50 mM Tris-HCl (pH 7.5), 10 mM 2-ME and 1 mg/ml 100T zymolyase) for 30-35 minutes [97]. Converted spheroplasts were washed once with cold zymolyase buffer without 2-ME, resuspended in nystatin buffer (final 50 mM NaCl, 1.5 mM $CaCl_2$, 20 mM Tris-HCl (pH 8.0), 1 M sorbitol, and 100 ug/ml nystatin (Sigma), and then kept on ice temporarily.

bioRxiv preprint doi: https://doi.org/10.1101/2020.12.20.423707; this version posted March 17, 2021. The copyright holder for this preprint (which was not certified by peer review) is the author/funder, who has granted bioRxiv a license to display the preprint in perpetuity. It is made available under aCC-BY-NC-ND 4.0 International license.

The following MNase digestion was performed for each strain individually. Resuspended spheroplasts were sequentially added into the MNase aliquots (ranged from final 0.0125 to 0.1 U/ml, prepared in nystatin buffer), and incubated at 25°C for 15 minutes. Reactions were stopped by adding 1% SDS/12 mM EDTA (final concentration) [98, 99]. Subsequently, the spheroplasts were treated with RNase (final 0.02 µg/µl) at 37°C for 45 minutes, followed by proteinase K (final 0.4 µg/µl) at 65°C, overnight. The DNA samples were purified with phenol/chloroform extraction, precipitated with ethanol overnight and then resuspended in 1X TE. The samples (2.5 µg) were analyzed with gel electrophoresis (1.2% TAE agarose gel, at 35 V overnight) [97].

Data availability

The datasets and computer code related to this study are available in the following databases:

- RNA-seq data: Gene Expression Omnibus 163287 (https//www.ncbi.nlm.nih.gov/geo/query/acc.cgi?acc=GSE163287)
- ChIP-seq data: Gene Expression Omnibus 42655 (https://www.ncbi.nlm.nih.gov/geo/query/acc.cgi?acc=GSE42655)

Acknowledgements

We thank K. Shirahige and Y. Katou for support and technical assistance during collection of the previously published ChIP-Seq data. We thank C. Björkegren for sharing strains and plasmids, and for critical reading of the manuscript.

bioRxiv preprint doi: https://doi.org/10.1101/2020.12.20.423707; this version posted March 17, 2021. The copyright holder for this preprint (which was not certified by peer review) is the author/funder, who has granted bioRxiv a license to display the preprint in perpetuity. It is made available under aCC-BY-NC-ND 4.0 International license.

Conflict of interest

The authors declare that they have no conflict of interest.

References

1. Terweij M, van Leeuwen F. Histone exchange: sculpting the epigenome. Frontiers in Life Science. 2013;7(1-2):63-79. doi: 10.1080/21553769.2013.838193.
2. Venkatesh S, Workman JL. Histone exchange, chromatin structure and the regulation of transcription. Nature reviews Molecular cell biology. 2015;16(3):178-89. doi: 10.1038/nrm3941. PubMed PMID: 25650798.
3. Lengronne A, Katou Y, Mori S, Yokobayashi S, Kelly GP, Itoh T, et al. Cohesin relocation from sites of chromosomal loading to places of convergent transcription. Nature. 2004;430(6999):573-8. doi: 10.1038/nature02742. PubMed PMID: 15229615; PubMed Central PMCID: PMC2610358.
4. Glynn EF, Megee PC, Yu HG, Mistrot C, Unal E, Koshland DE, et al. Genome-wide mapping of the cohesin complex in the yeast Saccharomyces cerevisiae. PLoS Biol. 2004;2(9):E259. Epub 2004/08/17. doi: 10.1371/journal.pbio.0020259. PubMed PMID: 15309048; PubMed Central PMCID: PMCPMC490026.
5. Dorsett D, Strom L. The ancient and evolving roles of cohesin in gene expression and DNA repair. Current biology : CB. 2012;22(7):R240-50. doi: 10.1016/j.cub.2012.02.046. PubMed PMID: 22497943; PubMed Central PMCID: PMC3327610.
6. Lopez-Serra L, Kelly G, Patel H, Stewart A, Uhlmann F. The Scc2-Scc4 complex acts in sister chromatid cohesion and transcriptional regulation by maintaining nucleosome-free regions. Nat Genet. 2014;46(10):1147-51. Epub 2014/09/01. doi: 10.1038/ng.3080. PubMed PMID: 25173104; PubMed Central PMCID: PMCPMC4177232.
7. Lindgren E, Hagg S, Giordano F, Bjorkegren J, Strom L. Inactivation of the budding yeast cohesin loader Scc2 alters gene expression both globally and in response to a single DNA double strand break. Cell cycle. 2014;13(23):3645-58. doi: 10.4161/15384101.2014.964108. PubMed PMID: 25483075; PubMed Central PMCID: PMC4612677.
8. Lazar-Stefanita L, Scolari VF, Mercy G, Muller H, Guerin TM, Thierry A, et al. Cohesins and condensins orchestrate the 4D dynamics of yeast chromosomes during the cell cycle. The EMBO journal. 2017;36(18):2684-97. doi: 10.15252/embj.201797342. PubMed PMID: 28729434; PubMed Central PMCID: PMC5599795.
9. Haarhuis JHI, van der Weide RH, Blomen VA, Yanez-Cuna JO, Amendola M, van Ruiten MS, et al. The Cohesin Release Factor WAPL Restricts Chromatin Loop Extension. Cell. 2017;169(4):693-707 e14. doi: 10.1016/j.cell.2017.04.013. PubMed PMID: 28475897; PubMed Central PMCID: PMC5422210.
10. Schalbetter SA, Goloborodko A, Fudenberg G, Belton JM, Miles C, Yu M, et al. SMC complexes differentially compact mitotic chromosomes according to genomic context. Nature cell biology. 2017;19(9):1071-80. doi: 10.1038/ncb3594. PubMed PMID: 28825700; PubMed Central PMCID: PMC5640152.
11. Davidson IF, Bauer B, Goetz D, Tang W, Wutz G, Peters JM. DNA loop extrusion by human cohesin. Science. 2019;366(6471):1338-45. doi: 10.1126/science.aaz3418. PubMed PMID: 31753851.

bioRxiv preprint doi: https://doi.org/10.1101/2020.12.20.423707; this version posted March 17, 2021. The copyright holder for this preprint (which was not certified by peer review) is the author/funder, who has granted bioRxiv a license to display the preprint in perpetuity. It is made available under aCC-BY-NC-ND 4.0 International license.

12. Kim Y, Shi Z, Zhang H, Finkelstein IJ, Yu H. Human cohesin compacts DNA by loop extrusion. Science. 2019;366(6471):1345-9. doi: 10.1126/science.aaz4475. PubMed PMID: 31780627; PubMed Central PMCID: PMC7387118.
13. Ciosk R, Shirayama M, Shevchenko A, Tanaka T, Toth A, Shevchenko A, et al. Cohesin's binding to chromosomes depends on a separate complex consisting of Scc2 and Scc4 proteins. Molecular cell. 2000;5(2):243-54. doi: 10.1016/s1097-2765(00)80420-7. PubMed PMID: 10882066.
14. Srinivasan M, Fumasoni M, Petela NJ, Murray A, Nasmyth KA. Cohesion is established during DNA replication utilising chromosome associated cohesin rings as well as those loaded de novo onto nascent DNAs. eLife. 2020;9. doi: 10.7554/eLife.56611. PubMed PMID: 32515737; PubMed Central PMCID: PMC7282809.
15. Uhlmann F, Nasmyth K. Cohesion between sister chromatids must be established during DNA replication. Curr Biol. 1998;8(20):1095-101. Epub 1998/10/21. doi: 10.1016/s0960-9822(98)70463-4. PubMed PMID: 9778527.
16. Rolef Ben-Shahar T, Heeger S, Lehane C, East P, Flynn H, Skehel M, et al. Eco1-dependent cohesin acetylation during establishment of sister chromatid cohesion. Science. 2008;321(5888):563-6. Epub 2008/07/26. doi: 10.1126/science.1157774. PubMed PMID: 18653893.
17. Unal E, Heidinger-Pauli JM, Kim W, Guacci V, Onn I, Gygi SP, et al. A molecular determinant for the establishment of sister chromatid cohesion. Science. 2008;321(5888):566-9. Epub 2008/07/26. doi: 10.1126/science.1157880. PubMed PMID: 18653894.
18. Zhang J, Shi X, Li Y, Kim BJ, Jia J, Huang Z, et al. Acetylation of Smc3 by Eco1 is required for S phase sister chromatid cohesion in both human and yeast. Mol Cell. 2008;31(1):143-51. Epub 2008/07/11. doi: 10.1016/j.molcel.2008.06.006. PubMed PMID: 18614053.
19. Uhlmann F, Lottspeich F, Nasmyth K. Sister-chromatid separation at anaphase onset is promoted by cleavage of the cohesin subunit Scc1. Nature. 1999;400(6739):37-42. Epub 1999/07/14. doi: 10.1038/21831. PubMed PMID: 10403247.
20. Lyons NA, Fonslow BR, Diedrich JK, Yates JR, 3rd, Morgan DO. Sequential primed kinases create a damage-responsive phosphodegron on Eco1. Nat Struct Mol Biol. 2013;20(2):194-201. Epub 2013/01/15. doi: 10.1038/nsmb.2478. PubMed PMID: 23314252; PubMed Central PMCID: PMCPMC3565030.
21. Lyons NA, Morgan DO. Cdk1-dependent destruction of Eco1 prevents cohesion establishment after S phase. Molecular cell. 2011;42(3):378-89. doi: 10.1016/j.molcel.2011.03.023. PubMed PMID: 21549314; PubMed Central PMCID: PMC3095509.
22. Unal E, Heidinger-Pauli JM, Koshland D. DNA double-strand breaks trigger genome-wide sister-chromatid cohesion through Eco1 (Ctf7). Science. 2007;317(5835):245-8. Epub 2007/07/14. doi: 10.1126/science.1140637. PubMed PMID: 17626885.
23. Strom L, Lindroos HB, Shirahige K, Sjogren C. Postreplicative recruitment of cohesin to double-strand breaks is required for DNA repair. Molecular cell. 2004;16(6):1003-15. doi: 10.1016/j.molcel.2004.11.026. PubMed PMID: 15610742.
24. Strom L, Karlsson C, Lindroos HB, Wedahl S, Katou Y, Shirahige K, et al. Postreplicative formation of cohesion is required for repair and induced by a single DNA break. Science. 2007;317(5835):242-5. Epub 2007/07/14. doi: 10.1126/science.1140649. PubMed PMID: 17626884.
25. Enervald E, Lindgren E, Katou Y, Shirahige K, Strom L. Importance of Poleta for damage-induced cohesion reveals differential regulation of cohesion establishment at the break site and genome-wide. PLoS Genet. 2013;9(1):e1003158. Epub 2013/01/18. doi: 10.1371/journal.pgen.1003158. PubMed PMID: 23326240; PubMed Central PMCID: PMCPMC3542068.
26. Johnson RE, Prakash S, Prakash L. Efficient bypass of a thymine-thymine dimer by yeast DNA polymerase, Poleta. Science. 1999;283(5404):1001-4. doi: 10.1126/science.283.5404.1001. PubMed PMID: 9974380.
27. Acharya N, Manohar K, Peroumal D, Khandagale P, Patel SK, Sahu SR, et al. Multifaceted activities of DNA polymerase eta: beyond translesion DNA synthesis. Curr Genet. 2019;65(3):649-56. Epub 2018/12/12. doi: 10.1007/s00294-018-0918-5. PubMed PMID: 30535880.

bioRxiv preprint doi: https://doi.org/10.1101/2020.12.20.423707; this version posted March 17, 2021. The copyright holder for this preprint (which was not certified by peer review) is the author/funder, who has granted bioRxiv a license to display the preprint in perpetuity. It is made available under aCC-BY-NC-ND 4.0 International license.

28. Wu PS, Enervald E, Joelsson A, Palmberg C, Rutishauser D, Hallberg BM, et al. Post-translational Regulation of DNA Polymerase eta, a Connection to Damage-Induced Cohesion in Saccharomyces cerevisiae. Genetics. 2020;216(4):1009-22. Epub 2020/10/10. doi: 10.1534/genetics.120.303494. PubMed PMID: 33033113; PubMed Central PMCID: PMCPMC7768261.
29. Gali VK, Balint E, Serbyn N, Frittmann O, Stutz F, Unk I. Translesion synthesis DNA polymerase eta exhibits a specific RNA extension activity and a transcription-associated function. Sci Rep. 2017;7(1):13055. Epub 2017/10/14. doi: 10.1038/s41598-017-12915-1. PubMed PMID: 29026143; PubMed Central PMCID: PMCPMC5638924.
30. Bhardwaj S, Schlackow M, Rabajdova M, Gullerova M. Transcription facilitates sister chromatid cohesion on chromosomal arms. Nucleic acids research. 2016;44(14):6676-92. doi: 10.1093/nar/gkw252. PubMed PMID: 27084937; PubMed Central PMCID: PMC5001582.
31. Desmoucelles C, Pinson B, Saint-Marc C, Daignan-Fornier B. Screening the yeast "disruptome" for mutants affecting resistance to the immunosuppressive drug, mycophenolic acid. The Journal of biological chemistry. 2002;277(30):27036-44. doi: 10.1074/jbc.M111433200. PubMed PMID: 12016207.
32. McKay BC, Stubbert LJ, Fowler CC, Smith JM, Cardamore RA, Spronck JC. Regulation of ultraviolet light-induced gene expression by gene size. Proceedings of the National Academy of Sciences of the United States of America. 2004;101(17):6582-6. doi: 10.1073/pnas.0308181101. PubMed PMID: 15087501; PubMed Central PMCID: PMC404088.
33. Williamson L, Saponaro M, Boeing S, East P, Mitter R, Kantidakis T, et al. UV Irradiation Induces a Non-coding RNA that Functionally Opposes the Protein Encoded by the Same Gene. Cell. 2017;168(5):843-55 e13. doi: 10.1016/j.cell.2017.01.019. PubMed PMID: 28215706; PubMed Central PMCID: PMC5332558.
34. Maya-Miles D, Andujar E, Perez-Alegre M, Murillo-Pineda M, Barrientos-Moreno M, Cabello-Lobato MJ, et al. Crosstalk between chromatin structure, cohesin activity and transcription. Epigenetics & chromatin. 2019;12(1):47. doi: 10.1186/s13072-019-0293-6. PubMed PMID: 31331360; PubMed Central PMCID: PMC6647288.
35. Zaugg JB, Luscombe NM. A genomic model of condition-specific nucleosome behavior explains transcriptional activity in yeast. Genome research. 2012;22(1):84-94. doi: 10.1101/gr.124099.111. PubMed PMID: 21930892; PubMed Central PMCID: PMC3246209.
36. Kubik S, Bruzzone MJ, Jacquet P, Falcone JL, Rougemont J, Shore D. Nucleosome Stability Distinguishes Two Different Promoter Types at All Protein-Coding Genes in Yeast. Molecular cell. 2015;60(3):422-34. doi: 10.1016/j.molcel.2015.10.002. PubMed PMID: 26545077.
37. Basehoar AD, Zanton SJ, Pugh BF. Identification and distinct regulation of yeast TATA box-containing genes. Cell. 2004;116(5):699-709. doi: 10.1016/s0092-8674(04)00205-3. PubMed PMID: 15006352.
38. Huisinga KL, Pugh BF. A genome-wide housekeeping role for TFIID and a highly regulated stress-related role for SAGA in Saccharomyces cerevisiae. Molecular cell. 2004;13(4):573-85. doi: 10.1016/s1097-2765(04)00087-5. PubMed PMID: 14992726.
39. Bausch C, Noone S, Henry JM, Gaudenz K, Sanderson B, Seidel C, et al. Transcription alters chromosomal locations of cohesin in Saccharomyces cerevisiae. Molecular and cellular biology. 2007;27(24):8522-32. doi: 10.1128/MCB.01007-07. PubMed PMID: 17923700; PubMed Central PMCID: PMC2169412.
40. Prochasson P, Florens L, Swanson SK, Washburn MP, Workman JL. The HIR corepressor complex binds to nucleosomes generating a distinct protein/DNA complex resistant to remodeling by SWI/SNF. Genes & development. 2005;19(21):2534-9. doi: 10.1101/gad.1341105. PubMed PMID: 16264190; PubMed Central PMCID: PMC1276727.
41. Green EM, Antczak AJ, Bailey AO, Franco AA, Wu KJ, Yates JR, 3rd, et al. Replication-independent histone deposition by the HIR complex and Asf1. Current biology : CB. 2005;15(22):2044-9. doi: 10.1016/j.cub.2005.10.053. PubMed PMID: 16303565; PubMed Central PMCID: PMC2819815.

bioRxiv preprint doi: https://doi.org/10.1101/2020.12.20.423707; this version posted March 17, 2021. The copyright holder for this preprint (which was not certified by peer review) is the author/funder, who has granted bioRxiv a license to display the preprint in perpetuity. It is made available under aCC-BY-NC-ND 4.0 International license.

42. Rufiange A, Jacques PE, Bhat W, Robert F, Nourani A. Genome-wide replication-independent histone H3 exchange occurs predominantly at promoters and implicates H3 K56 acetylation and Asf1. Molecular cell. 2007;27(3):393-405. doi: 10.1016/j.molcel.2007.07.011. PubMed PMID: 17679090.
43. Dion MF, Kaplan T, Kim M, Buratowski S, Friedman N, Rando OJ. Dynamics of replication-independent histone turnover in budding yeast. Science. 2007;315(5817):1405-8. doi: 10.1126/science.1134053. PubMed PMID: 17347438.
44. Sherwood PW, Tsang SV, Osley MA. Characterization of HIR1 and HIR2, two genes required for regulation of histone gene transcription in Saccharomyces cerevisiae. Molecular and cellular biology. 1993;13(1):28-38. doi: 10.1128/mcb.13.1.28. PubMed PMID: 8417331; PubMed Central PMCID: PMC358881.
45. Osley MA, Lycan D. Trans-acting regulatory mutations that alter transcription of Saccharomyces cerevisiae histone genes. Molecular and cellular biology. 1987;7(12):4204-10. doi: 10.1128/mcb.7.12.4204. PubMed PMID: 3125420; PubMed Central PMCID: PMC368101.
46. Zhang H, Roberts DN, Cairns BR. Genome-wide dynamics of Htz1, a histone H2A variant that poises repressed/basal promoters for activation through histone loss. Cell. 2005;123(2):219-31. doi: 10.1016/j.cell.2005.08.036. PubMed PMID: 16239141; PubMed Central PMCID: PMC2788555.
47. Li B, Pattenden SG, Lee D, Gutierrez J, Chen J, Seidel C, et al. Preferential occupancy of histone variant H2AZ at inactive promoters influences local histone modifications and chromatin remodeling. Proceedings of the National Academy of Sciences of the United States of America. 2005;102(51):18385-90. doi: 10.1073/pnas.0507975102. PubMed PMID: 16344463; PubMed Central PMCID: PMC1317944.
48. Weber CM, Ramachandran S, Henikoff S. Nucleosomes are context-specific, H2A.Z-modulated barriers to RNA polymerase. Molecular cell. 2014;53(5):819-30. doi: 10.1016/j.molcel.2014.02.014. PubMed PMID: 24606920.
49. Rhee HS, Bataille AR, Zhang L, Pugh BF. Subnucleosomal structures and nucleosome asymmetry across a genome. Cell. 2014;159(6):1377-88. doi: 10.1016/j.cell.2014.10.054. PubMed PMID: 25480300; PubMed Central PMCID: PMC4258235.
50. Morillo-Huesca M, Clemente-Ruiz M, Andujar E, Prado F. The SWR1 histone replacement complex causes genetic instability and genome-wide transcription misregulation in the absence of H2A.Z. PloS one. 2010;5(8):e12143. doi: 10.1371/journal.pone.0012143. PubMed PMID: 20711347; PubMed Central PMCID: PMC2920830.
51. Sharma U, Stefanova D, Holmes SG. Histone variant H2A.Z functions in sister chromatid cohesion in Saccharomyces cerevisiae. Molecular and cellular biology. 2013;33(17):3473-81. doi: 10.1128/MCB.00162-12. PubMed PMID: 23816883; PubMed Central PMCID: PMC3753853.
52. Govind CK, Qiu H, Ginsburg DS, Ruan C, Hofmeyer K, Hu C, et al. Phosphorylated Pol II CTD recruits multiple HDACs, including Rpd3C(S), for methylation-dependent deacetylation of ORF nucleosomes. Molecular cell. 2010;39(2):234-46. doi: 10.1016/j.molcel.2010.07.003. PubMed PMID: 20670892; PubMed Central PMCID: PMC2937259.
53. Ruan C, Lee CH, Cui H, Li S, Li B. Nucleosome contact triggers conformational changes of Rpd3S driving high-affinity H3K36me nucleosome engagement. Cell reports. 2015;10(2):204-15. doi: 10.1016/j.celrep.2014.12.027. PubMed PMID: 25578729; PubMed Central PMCID: PMC4359074.
54. Venkatesh S, Smolle M, Li H, Gogol MM, Saint M, Kumar S, et al. Set2 methylation of histone H3 lysine 36 suppresses histone exchange on transcribed genes. Nature. 2012;489(7416):452-5. doi: 10.1038/nature11326. PubMed PMID: 22914091.
55. Strahl BD, Grant PA, Briggs SD, Sun ZW, Bone JR, Caldwell JA, et al. Set2 is a nucleosomal histone H3-selective methyltransferase that mediates transcriptional repression. Molecular and cellular biology. 2002;22(5):1298-306. doi: 10.1128/mcb.22.5.1298-1306.2002. PubMed PMID: 11839797; PubMed Central PMCID: PMC134702.
56. Landry J, Sutton A, Hesman T, Min J, Xu RM, Johnston M, et al. Set2-catalyzed methylation of histone H3 represses basal expression of GAL4 in Saccharomyces cerevisiae. Molecular and cellular biology. 2003;23(17):5972-8. doi: 10.1128/mcb.23.17.5972-5978.2003. PubMed PMID: 12917322; PubMed Central PMCID: PMC180946.

bioRxiv preprint doi: https://doi.org/10.1101/2020.12.20.423707; this version posted March 17, 2021. The copyright holder for this preprint (which was not certified by peer review) is the author/funder, who has granted bioRxiv a license to display the preprint in perpetuity. It is made available under aCC-BY-NC-ND 4.0 International license.

57. Biswas D, Dutta-Biswas R, Mitra D, Shibata Y, Strahl BD, Formosa T, et al. Opposing roles for Set2 and yFACT in regulating TBP binding at promoters. The EMBO journal. 2006;25(19):4479-89. doi: 10.1038/sj.emboj.7601333. PubMed PMID: 16977311; PubMed Central PMCID: PMC1589996.
58. Exinger F, Lacroute F. 6-Azauracil inhibition of GTP biosynthesis in Saccharomyces cerevisiae. Current genetics. 1992;22(1):9-11. doi: 10.1007/BF00351735. PubMed PMID: 1611672.
59. Franklin TJ, Cook JM. The inhibition of nucleic acid synthesis by mycophenolic acid. The Biochemical journal. 1969;113(3):515-24. doi: 10.1042/bj1130515. PubMed PMID: 5807210; PubMed Central PMCID: PMC1184694.
60. Kizer KO, Phatnani HP, Shibata Y, Hall H, Greenleaf AL, Strahl BD. A novel domain in Set2 mediates RNA polymerase II interaction and couples histone H3 K36 methylation with transcript elongation. Molecular and cellular biology. 2005;25(8):3305-16. doi: 10.1128/MCB.25.8.3305-3316.2005. PubMed PMID: 15798214; PubMed Central PMCID: PMC1069628.
61. Trask DK, Muller MT. Stabilization of type I topoisomerase-DNA covalent complexes by actinomycin D. Proceedings of the National Academy of Sciences of the United States of America. 1988;85(5):1417-21. doi: 10.1073/pnas.85.5.1417. PubMed PMID: 2830618; PubMed Central PMCID: PMC279782.
62. Bi X, Yu Q, Siler J, Li C, Khan A. Functions of Fun30 chromatin remodeler in regulating cellular resistance to genotoxic stress. PloS one. 2015;10(3):e0121341. doi: 10.1371/journal.pone.0121341. PubMed PMID: 25806814; PubMed Central PMCID: PMC4373758.
63. Segovia R, Shen Y, Lujan SA, Jones SJ, Stirling PC. Hypermutation signature reveals a slippage and realignment model of translesion synthesis by Rev3 polymerase in cisplatin-treated yeast. Proceedings of the National Academy of Sciences of the United States of America. 2017;114(10):2663-8. doi: 10.1073/pnas.1618555114. PubMed PMID: 28223526; PubMed Central PMCID: PMC5347559.
64. Galdieri L, Zhang T, Rogerson D, Vancura A. Reduced Histone Expression or a Defect in Chromatin Assembly Induces Respiration. Molecular and cellular biology. 2016;36(7):1064-77. doi: 10.1128/MCB.00770-15. PubMed PMID: 26787838; PubMed Central PMCID: PMC4800798.
65. Sharp JA, Franco AA, Osley MA, Kaufman PD. Chromatin assembly factor I and Hir proteins contribute to building functional kinetochores in S. cerevisiae. Genes & development. 2002;16(1):85-100. doi: 10.1101/gad.925302. PubMed PMID: 11782447; PubMed Central PMCID: PMC155315.
66. Kaufman PD, Cohen JL, Osley MA. Hir proteins are required for position-dependent gene silencing in Saccharomyces cerevisiae in the absence of chromatin assembly factor I. Molecular and cellular biology. 1998;18(8):4793-806. doi: 10.1128/mcb.18.8.4793. PubMed PMID: 9671489; PubMed Central PMCID: PMC109065.
67. Lai WKM, Pugh BF. Understanding nucleosome dynamics and their links to gene expression and DNA replication. Nature reviews Molecular cell biology. 2017;18(9):548-62. doi: 10.1038/nrm.2017.47. PubMed PMID: 28537572; PubMed Central PMCID: PMC5831138.
68. Hsieh TH, Weiner A, Lajoie B, Dekker J, Friedman N, Rando OJ. Mapping Nucleosome Resolution Chromosome Folding in Yeast by Micro-C. Cell. 2015;162(1):108-19. doi: 10.1016/j.cell.2015.05.048. PubMed PMID: 26119342; PubMed Central PMCID: PMC4509605.
69. van Steensel B, Furlong EEM. The role of transcription in shaping the spatial organization of the genome. Nature reviews Molecular cell biology. 2019;20(6):327-37. doi: 10.1038/s41580-019-0114-6. PubMed PMID: 30886333; PubMed Central PMCID: PMC7116054.
70. Lengronne A, McIntyre J, Katou Y, Kanoh Y, Hopfner KP, Shirahige K, et al. Establishment of sister chromatid cohesion at the S. cerevisiae replication fork. Molecular cell. 2006;23(6):787-99. doi: 10.1016/j.molcel.2006.08.018. PubMed PMID: 16962805.
71. Zhang J, Shi D, Li X, Ding L, Tang J, Liu C, et al. Rtt101-Mms1-Mms22 coordinates replication-coupled sister chromatid cohesion and nucleosome assembly. EMBO reports. 2017;18(8):1294-305. doi: 10.15252/embr.201643807. PubMed PMID: 28615292; PubMed Central PMCID: PMC5538422.
72. Dion V, Kalck V, Horigome C, Towbin BD, Gasser SM. Increased mobility of double-strand breaks requires Mec1, Rad9 and the homologous recombination machinery. Nature cell biology. 2012;14(5):502-9. doi: 10.1038/ncb2465. PubMed PMID: 22484486.

bioRxiv preprint doi: https://doi.org/10.1101/2020.12.20.423707; this version posted March 17, 2021. The copyright holder for this preprint (which was not certified by peer review) is the author/funder, who has granted bioRxiv a license to display the preprint in perpetuity. It is made available under aCC-BY-NC-ND 4.0 International license.

73. Mine-Hattab J, Rothstein R. Increased chromosome mobility facilitates homology search during recombination. Nature cell biology. 2012;14(5):510-7. doi: 10.1038/ncb2472. PubMed PMID: 22484485.
74. Dion V, Kalck V, Seeber A, Schleker T, Gasser SM. Cohesin and the nucleolus constrain the mobility of spontaneous repair foci. EMBO reports. 2013;14(11):984-91. doi: 10.1038/embor.2013.142. PubMed PMID: 24018421; PubMed Central PMCID: PMC3818071.
75. Sagot I, Schaeffer J, Daignan-Fornier B. Guanylic nucleotide starvation affects Saccharomyces cerevisiae mother-daughter separation and may be a signal for entry into quiescence. BMC cell biology. 2005;6(1):24. doi: 10.1186/1471-2121-6-24. PubMed PMID: 15869715; PubMed Central PMCID: PMC1274246.
76. Kushnirov VV. Rapid and reliable protein extraction from yeast. Yeast. 2000;16(9):857-60. doi: 10.1002/1097-0061(20000630)16:9<857::AID-YEA561>3.0.CO;2-B. PubMed PMID: 10861908.
77. Martin M. Cutadapt removes adapter sequences from high-throughput sequencing reads. 2011. 2011;17(1):3. Epub 2011-08-02. doi: 10.14806/ej.17.1.200.
78. Kim D, Paggi JM, Park C, Bennett C, Salzberg SL. Graph-based genome alignment and genotyping with HISAT2 and HISAT-genotype. Nature biotechnology. 2019;37(8):907-15. doi: 10.1038/s41587-019-0201-4. PubMed PMID: 31375807; PubMed Central PMCID: PMC7605509.
79. Langmead B, Trapnell C, Pop M, Salzberg SL. Ultrafast and memory-efficient alignment of short DNA sequences to the human genome. Genome biology. 2009;10(3):R25. doi: 10.1186/gb-2009-10-3-r25. PubMed PMID: 19261174; PubMed Central PMCID: PMC2690996.
80. Li H, Durbin R. Fast and accurate short read alignment with Burrows-Wheeler transform. Bioinformatics. 2009;25(14):1754-60. doi: 10.1093/bioinformatics/btp324. PubMed PMID: 19451168; PubMed Central PMCID: PMC2705234.
81. Liao Y, Smyth GK, Shi W. featureCounts: an efficient general purpose program for assigning sequence reads to genomic features. Bioinformatics. 2014;30(7):923-30. doi: 10.1093/bioinformatics/btt656. PubMed PMID: 24227677.
82. McCarthy DJ, Chen Y, Smyth GK. Differential expression analysis of multifactor RNA-Seq experiments with respect to biological variation. Nucleic acids research. 2012;40(10):4288-97. doi: 10.1093/nar/gks042. PubMed PMID: 22287627; PubMed Central PMCID: PMC3378882.
83. Robinson MD, McCarthy DJ, Smyth GK. edgeR: a Bioconductor package for differential expression analysis of digital gene expression data. Bioinformatics. 2010;26(1):139-40. doi: 10.1093/bioinformatics/btp616. PubMed PMID: 19910308; PubMed Central PMCID: PMC2796818.
84. Love MI, Huber W, Anders S. Moderated estimation of fold change and dispersion for RNA-seq data with DESeq2. Genome biology. 2014;15(12):550. doi: 10.1186/s13059-014-0550-8. PubMed PMID: 25516281; PubMed Central PMCID: PMC4302049.
85. Zhang Y, Liu T, Meyer CA, Eeckhoute J, Johnson DS, Bernstein BE, et al. Model-based analysis of ChIP-Seq (MACS). Genome biology. 2008;9(9):R137. doi: 10.1186/gb-2008-9-9-r137. PubMed PMID: 18798982; PubMed Central PMCID: PMC2592715.
86. Zhu LJ, Gazin C, Lawson ND, Pages H, Lin SM, Lapointe DS, et al. ChIPpeakAnno: a Bioconductor package to annotate ChIP-seq and ChIP-chip data. BMC bioinformatics. 2010;11:237. doi: 10.1186/1471-2105-11-237. PubMed PMID: 20459804; PubMed Central PMCID: PMC3098059.
87. Durinck S, Spellman PT, Birney E, Huber W. Mapping identifiers for the integration of genomic datasets with the R/Bioconductor package biomaRt. Nature protocols. 2009;4(8):1184-91. doi: 10.1038/nprot.2009.97. PubMed PMID: 19617889; PubMed Central PMCID: PMC3159387.
88. Shen L, Shao N, Liu X, Nestler E. ngs.plot: Quick mining and visualization of next-generation sequencing data by integrating genomic databases. BMC genomics. 2014;15:284. doi: 10.1186/1471-2164-15-284. PubMed PMID: 24735413; PubMed Central PMCID: PMC4028082.
89. Subramanian A, Tamayo P, Mootha VK, Mukherjee S, Ebert BL, Gillette MA, et al. Gene set enrichment analysis: a knowledge-based approach for interpreting genome-wide expression profiles. Proceedings of the National Academy of Sciences of the United States of America. 2005;102(43):15545-50. doi: 10.1073/pnas.0506580102. PubMed PMID: 16199517; PubMed Central PMCID: PMC1239896.

bioRxiv preprint doi: https://doi.org/10.1101/2020.12.20.423707; this version posted March 17, 2021. The copyright holder for this preprint (which was not certified by peer review) is the author/funder, who has granted bioRxiv a license to display the preprint in perpetuity. It is made available under aCC-BY-NC-ND 4.0 International license.

90. Lai L, Hennessey J, Bares V, Son EW, Ban Y, Wang W, et al. GSKB: A gene set database for pathway analysis in mouse. bioRxiv. 2016:082511. doi: 10.1101/082511.
91. Merico D, Isserlin R, Stueker O, Emili A, Bader GD. Enrichment map: a network-based method for gene-set enrichment visualization and interpretation. PloS one. 2010;5(11):e13984. doi: 10.1371/journal.pone.0013984. PubMed PMID: 21085593; PubMed Central PMCID: PMC2981572.
92. Shannon P, Markiel A, Ozier O, Baliga NS, Wang JT, Ramage D, et al. Cytoscape: a software environment for integrated models of biomolecular interaction networks. Genome research. 2003;13(11):2498-504. doi: 10.1101/gr.1239303. PubMed PMID: 14597658; PubMed Central PMCID: PMC403769.
93. Reimand J, Isserlin R, Voisin V, Kucera M, Tannus-Lopes C, Rostamianfar A, et al. Pathway enrichment analysis and visualization of omics data using g:Profiler, GSEA, Cytoscape and EnrichmentMap. Nature protocols. 2019;14(2):482-517. doi: 10.1038/s41596-018-0103-9. PubMed PMID: 30664679; PubMed Central PMCID: PMC6607905.
94. Kucera M, Isserlin R, Arkhangorodsky A, Bader GD. AutoAnnotate: A Cytoscape app for summarizing networks with semantic annotations. F1000Research. 2016;5:1717. doi: 10.12688/f1000research.9090.1. PubMed PMID: 27830058; PubMed Central PMCID: PMC5082607.
95. Krogan NJ, Baetz K, Keogh MC, Datta N, Sawa C, Kwok TC, et al. Regulation of chromosome stability by the histone H2A variant Htz1, the Swr1 chromatin remodeling complex, and the histone acetyltransferase NuA4. Proceedings of the National Academy of Sciences of the United States of America. 2004;101(37):13513-8. doi: 10.1073/pnas.0405753101. PubMed PMID: 15353583; PubMed Central PMCID: PMC518788.
96. Sjogren C, Nasmyth K. Sister chromatid cohesion is required for postreplicative double-strand break repair in Saccharomyces cerevisiae. Current biology : CB. 2001;11(12):991-5. doi: 10.1016/s0960-9822(01)00271-8. PubMed PMID: 11448778.
97. Lantermann A, Stralfors A, Fagerstrom-Billai F, Korber P, Ekwall K. Genome-wide mapping of nucleosome positions in Schizosaccharomyces pombe. Methods. 2009;48(3):218-25. doi: 10.1016/j.ymeth.2009.02.004. PubMed PMID: 19233281.
98. Venditti S, Camilloni G. In vivo analysis of chromatin following nystatin-mediated import of active enzymes into Saccharomyces cerevisiae. Molecular & general genetics : MGG. 1994;242(1):100-4. doi: 10.1007/BF00277353. PubMed PMID: 8277940.
99. Celona B, Weiner A, Di Felice F, Mancuso FM, Cesarini E, Rossi RL, et al. Substantial histone reduction modulates genomewide nucleosomal occupancy and global transcriptional output. PLoS biology. 2011;9(6):e1001086. doi: 10.1371/journal.pbio.1001086. PubMed PMID: 21738444; PubMed Central PMCID: PMC3125158.

bioRxiv preprint doi: https://doi.org/10.1101/2020.12.20.423707; this version posted March 17, 2021. The copyright holder for this preprint (which was not certified by peer review) is the author/funder, who has granted bioRxiv a license to display the preprint in perpetuity. It is made available under aCC-BY-NC-ND 4.0 International license.

Figure legends

Fig 1. A potential role for Polη in facilitating chromatin association of RNAPII

(A) Spot assay to monitor sensitivity of the *rad30Δ* and *Polη-S14A* mutants to the transcription elongation inhibitors, actinomycin D and mycophenolic acid (MPA). Tenfold serial dilutions of indicated mid-log phase cells on controls (-Ura plate ± guanine), and drug-containing plates, after 3 days incubation at room temperature. (B) ChIP-qPCR analyses to determine chromatin association of Rpb1 in indicated strains, on selected actively transcribed genes in G_2/M arrested WT cells. Error bars indicate the mean ± STDEV of two independent experiments. Asterisks denote significant differences compared to the WT cells at indicated position ($p < 0.05$; One-way ANOVA, Tukey post hoc test). p, promoter; m, mid; e, end of gene body. n1 and n2, low-binding controls. (C-D) Western blot analysis of Rpb1 stability. G_2/M arrested cells from indicated strains, with or without one-hour P_{GAL}-*HO* break induction, were pelleted and resuspended in media containing cycloheximide (CHX) to monitor Rpb1 protein levels without further protein synthesis. Cdc11 was used as loading control. M, protein marker.

Fig 2. Transcription is perturbed in *rad30Δ* mutants

(A-C) Volcano plots showing differentially expressed genes between WT and *rad30Δ* cells, before and after DSB, determined by RNA-seq. Each dot represents one gene. Red and blue dots represent up- and down-regulated genes respectively. Numbers of differentially expressed genes are indicated. Black dots indicate genes without significant changes in expression ($p$adj < $-\text{Log}_{10}(0.5)$). $p$adj, adjusted p value. (D-E)

bioRxiv preprint doi: https://doi.org/10.1101/2020.12.20.423707; this version posted March 17, 2021. The copyright holder for this preprint (which was not certified by peer review) is the author/funder, who has granted bioRxiv a license to display the preprint in perpetuity. It is made available under aCC-BY-NC-ND 4.0 International license.

Comparisons between expression level of genes significantly up (D) or downregulated (E) in the WT+DSB relative to the G_2/M arrested WT cells, and expression of the same set of genes in the *rad30Δ* mutant, based on RNA-seq analysis. (F) Plot of fold change moving median, sorted by length (300 genes/window) to monitor the trend of gene expression after DSB in relation to gene length, comparing WT and *rad30Δ* cells. Fold change values were based on the changes of gene expression in WT and *rad30Δ* cells after DSB, determined by RNA-seq.

Fig 3. Increased cohesin binding around TSS in *rad30Δ* cells

(A) Metagenome plot showing cohesin enrichment ± 1000 bp from the transcription start site (TSS) in WT and *rad30Δ* cells ± DSB induction in G_2/M phase. The samples were first normalized to their respective input and then the values were scaled to the maximum value of the plot. (B) The data from (A) plotted relative to the WT-DSB sample. After normalizing to the input, all samples were also normalized to WT-DSB sample to visualize the changes between the WT and *rad30Δ* cells. (C) Metagenome plot showing cohesin distribution 1000 bp downstream and 100 bp upstream from the transcription end site (TES) in WT and *rad30Δ* cells ± DSB induction in G_2/M phase. Plotted as in (A). (D) As in (B), except plotting cohesin distribution around the TES according to (C).

bioRxiv preprint doi: https://doi.org/10.1101/2020.12.20.423707; this version posted March 17, 2021. The copyright holder for this preprint (which was not certified by peer review) is the author/funder, who has granted bioRxiv a license to display the preprint in perpetuity. It is made available under aCC-BY-NC-ND 4.0 International license.

Fig 4. Genes involved in chromatin assembly and positive transcription regulation pathways are downregulated in the absence of Polη

(A) Relatively enriched pathways in G_2/M arrested WT and *rad30Δ* cells, plotted with Cytoscape after gene set enrichment analysis (GSEA). The GSEA was performed with gene lists ranked by $\log_{10} p$ value (multiplied by the sign of the fold change) of each gene. The number of genes in each gene set is proportional to the circle size. Lines connect gene sets with similarity greater than 0.7. All gene sets have FDR < 0.05. (B) Gene set enrichment analysis after DSB induction, plotted with Cytoscape to depict the difference between WT and *rad30Δ* cells in up- or down-regulation of indicated pathways after DSB. Gene expression of WT and *rad30Δ* cells after DSB was compared to that of respective G_2/M arrested cells. GSEA was performed as in (A). The lines indicate the same as in (A). All gene sets have FDR < 0.05 and a normalized enrichment score > 2 for at least one of the WT or *rad30Δ* cells.

Fig 5. Deleting *HIR1* leads to partially deficient damage-induced cohesion

(A) Damage-induced cohesion assays of the *hir1Δ* single and *hir1Δrad30Δ* double mutants after P_{GAL}-*HO* induction, performed as illustrated in S4B Fig. Means ± STDEV from at least two independent experiments are shown. (B-C) Damage-induced cohesion assays of the *hhf1-hht1Δ* and *hht2-hhf2Δ* mutants after P_{GAL}-*HO* induction, performed as in (A). Means ± STDEV from at least two independent experiments are shown.

bioRxiv preprint doi: https://doi.org/10.1101/2020.12.20.423707; this version posted March 17, 2021. The copyright holder for this preprint (which was not certified by peer review) is the author/funder, who has granted bioRxiv a license to display the preprint in perpetuity. It is made available under aCC-BY-NC-ND 4.0 International license.

Fig 6. Perturbing histone exchange at promoters negatively affects formation of damage-induced cohesion

(A) Damage-induced cohesion assay of the *htz1Δ* mutant after γ-irradiation, performed according to the procedure described in the materials and methods. Means ± STDEV from at least two independent experiments are shown. (B-C) ChIP-qPCR analyses to determine Htz1 occupancy at promoters of selected genes, before (B) and (C) after DSB induction in G_2/M arrested WT and *rad30Δ* cells. *SPF1*, *RAD23* and *HAT2* are located at the left arm of chromosome V, where damage-induced cohesion was monitored. Error bars indicate the mean ± STDEV of at least two independent experiments. Asterisks denote significant differences compared to the WT cells ($p < 0.05$; t-Test). n, low-binding control.

Fig 7. The assisting role of Polη in transcription is needed for generation of damage-induced cohesion

(A) Spot assay to monitor the effect of *SET2* deletion on the *rad30Δ* mutant sensitivity to the transcription elongation inhibitors, actinomycin D and mycophenolic acid (MPA). Tenfold serial dilutions of indicated mid-log phase cells on control (-Ura plate ± guanine) and drug-containing plates, after 3 days incubation. (B) Damage-induced cohesion assay of the *set2Δ* mutant after P_{GAL}-*HO* induction, performed as depicted in S4B Fig. Means ± STDEV from at least two independent experiments are shown. (C-E) ChIP-qPCR analyses to determine chromatin association of Rpb1 at promoters and 3'-ends of selected genes, in indicated G_2/M arrested cells. Except *MSC1* and *NPL4*, the rest of the selected genes are located at the left arm of chromosome V, where damage-induced cohesion was monitored. Error bars indicate

bioRxiv preprint doi: https://doi.org/10.1101/2020.12.20.423707; this version posted March 17, 2021. The copyright holder for this preprint (which was not certified by peer review) is the author/funder, who has granted bioRxiv a license to display the preprint in perpetuity. It is made available under aCC-BY-NC-ND 4.0 International license.

the mean ± STDEV of at least two independent experiments. n, low-binding control (n2 in Fig 1B).

bioRxiv preprint doi: https://doi.org/10.1101/2020.12.20.423707; this version posted March 17, 2021. The copyright holder for this preprint (which was not certified by peer review) is the author/funder, who has granted bioRxiv a license to display the preprint in perpetuity. It is made available under aCC-BY-NC-ND 4.0 International license.

Supplementary figure legends

S1 Fig. Quantitation of Rpb1 levels

(A-B) Relative amounts of Rpb1 after addition of water (A, control) or galactose (B) to induce P_{GAL}-*HO* DSB induction for one-hour, followed by cycloheximide (CHX) chase up to 150 minutes. Western blots from two independent experiments were quantified to compare Rpb1 levels (relative to Cdc11) between the indicated strains.

S2 Fig. Control experiments for RNA-seq and a differential gene expression analysis in relation to cohesin binding

(A) FACS analysis to confirm benomyl-induced G_2/M arrest. 1G, 1-hour *GAL*-induction (P_{GAL}-*HO*). (B) PFGE analysis to monitor DSB induction on chromosome III. G2, G_2/M arrest; 1G as in (A). (C) PCA demonstrating distribution of independent data sets between groups and clustering of data sets within groups. (D) Venn diagrams showing overlaps of differentially expressed genes in WT and *rad30Δ* cells after DSB, based on RNA-seq. The red and blue arrows indicate up- and down-regulated genes respectively. Statistical significance of the overlapping genes was evaluated as described in Materials and Methods, with * $p < 0.001$. (E) Expression changes of short genes (< 500 bp) after DSB in WT and *rad30Δ* cells. Genes with or without cohesin enrichment were defined according to the Scc1 ChIP-seq data.

bioRxiv preprint doi: https://doi.org/10.1101/2020.12.20.423707; this version posted March 17, 2021. The copyright holder for this preprint (which was not certified by peer review) is the author/funder, who has granted bioRxiv a license to display the preprint in perpetuity. It is made available under aCC-BY-NC-ND 4.0 International license.

S3 Fig. The *rad30Δ* mutant showed increased nucleosome occupancy, but no difference in activation of DNA damage checkpoint and *ECO1* gene expression compared to WT cells

(A) Monitoring nucleosome occupancy based on sensitivity of cells to MNase digestions. The concentrations of MNase were 0, 0.0125, 0.025, 0.05, 0.1 U/ml (final). One representative gel electrophoresis from at least two independent assays performed is shown. The gel images were cropped to show selected samples. M, DNA ladder; Un, undigested; 1x, monomer; 2x, dimer; 3x, trimer; 4x, tetramer. (B) Monitoring activation of the DNA damage checkpoint (phosphorylation of Rad53) after DSB induction with western blot. Galactose was added into the G_2/M arrested cell cultures to induce P_{GAL}-*HO* break induction for 1- or 1.5-hour, denoted as 1G or 1.5G. Sample collected from G_2/M arrested WT cells, treated with phleomycin (final 15 μg/ml) for 1.5 hours was included as positive control (PC). Cdc11 was used as loading control. M, protein marker. (C) Monitoring activation of DNA damage checkpoint during DSB recovery. DSB was induced for 1- or 1.5-hour, as in (B). The cells were then allowed to recover in YEP media supplemented with glucose and benomyl for another 1.5 hour (1.5 R) at 35°C, to mimic the damage-induced cohesion assay. 1G, 1.5G, PC, M as in (B). Cdc11 was used as loading control. (D) FACS analyses of cell cycle progression in WT and *rad30Δ* cells, at indicated time points after release into YEP media supplemented with glucose to recover from DSB induction. Samples without DSBs were included as control. B, benomyl; R, recovery. (E) *ECO1* gene expression in G_2/M arrested WT and *rad30Δ* cells ± P_{GAL}-*HO* (left) and ± γ-irradiation (right). The relative gene expression was measured by RT-qPCR. *FBA1* was used as a reference gene for the ± P_{GAL}-*HO* samples. Purified total RNA (0.65 μg) was spiked in with 1 ng luciferase control RNA (Promega) prior to cDNA

bioRxiv preprint doi: https://doi.org/10.1101/2020.12.20.423707; this version posted March 17, 2021. The copyright holder for this preprint (which was not certified by peer review) is the author/funder, who has granted bioRxiv a license to display the preprint in perpetuity. It is made available under aCC-BY-NC-ND 4.0 International license.

synthesis for the ± γ-irradiation samples. Error bars indicate the mean ± STDEV of at least two independent experiments.

S4 Fig. The method and related control experiments for a typical damage-induced cohesion assay

(A) Detection of early DNA damage response (γ-H2AX) in thiolutin treated cells. G_2/M arrested WT cells were treated with 20 µg/ml thiolutin (final) for 20 minutes, denoted as 20'. The culture was then split for ± γ-irradiation, and allowed to recover for 30 minutes in the presence of thiolutin after ± γ-irradiation (30' R). Gamma-irradiated cells without thiolutin treatment were included as control. Cdc11 was used as loading control. M, protein marker. (B) Damage-induced cohesion assay performed with *GAL* induced DSBs on chromosome III (P_{GAL}-*HO*). Strains harboring the temperature sensitive *smc1-259* allele are arrested in G_2/M by addition of benomyl (B). Galactose is then added for expression of ectopic P_{GAL}-*SMC1-MYC* (Smc1 WT) and induction of DSBs, for 1-hour. The temperature is then raised to 35°C, restrictive to the *smc1-259* allele, for disruption of S-phase cohesion (blue rings). The Tet-O/TetR-GFP system (green dots) is used to monitor damage-induced cohesion (red rings) on chr. V. Chr., chromosome; III, three; V, five. B1 and 2 indicate replacement of media with freshly prepared benomyl. (C) FACS analysis to confirm G_2/M arrest during the time course of a typical damage-induced cohesion assay. 3B, 3-hour benomyl arrest. (D) PFGE analysis to detect DSB induction on chromosome III. 1, G_2/M arrest; 2, 1-hour *GAL*-induction (P_{GAL}-*HO* and P_{GAL}-*SMC1-MYC*). (E) Western blot to check expression of the *GAL* promoter driven ectopic Smc1-Myc protein. G2, G_2/M arrest; 1G, 1-hour *GAL*-induction as in (D). M and Cdc11 as in (A).

bioRxiv preprint doi: https://doi.org/10.1101/2020.12.20.423707; this version posted March 17, 2021. The copyright holder for this preprint (which was not certified by peer review) is the author/funder, who has granted bioRxiv a license to display the preprint in perpetuity. It is made available under aCC-BY-NC-ND 4.0 International license.

Fig S5. Damage-induced cohesion assay performed with γ-irradiation and the maintenance of sister chromatid cohesion in *htz1⊿* cells

(A) Damage-induced cohesion assay performed with γ-irradiation. Formation of damage-induced cohesion is monitored on chr. V with the same Tet-O/TetR-GFP system, as in S4B Fig, with slight differences in the experimental procedure. Strains with *smc1-259* background are arrested in G_2/M by addition of benomyl (B), expression of ectopic P_{GAL}-*SMC1-MYC* (Smc1 WT) is then induced by addition of galactose. The cells are subsequently pelleted, resuspended in 1X PBS supplemented with benomyl. The resuspension is split in one half for irradiation, and half as non-irradiated control. After irradiation, both ± irradiated cells are recovering in YEP media supplemented with galactose and benomyl. Subsequently, the media is changed to YEP containing glucose and benomyl, and the temperature raised to 35°C, to monitor formation of damage-induced cohesion. (B) Damage-induced cohesion assay of the *hir1Δ* mutant in response to γ-irradiation, performed as depicted in (A). Means ± STDEV from at least two independent experiments are shown. (C) Sister chromatid cohesion maintenance of the *htz1Δ* mutant under prolonged G_2/M arrest. The cells were initially synchronized in G_1 by α-factor in YEP media containing galactose. Expression of P_{GAL}-*CDC20* was then shut off by switching the carbon source to glucose (YEPD), which resulted in the subsequent prolonged G_2/M arrest as monitored by FACS (left panel). Sister chromatid separation was monitored at the *URA3* locus on Chr. V by the TetO/TetR-GFP system. Means ± STDEV from at least two independent experiments are shown (right panel). A *rad61Δ* mutant with known high sister separation under prolonged G_2/M arrest was included as control. Means ± STDEV from at least two independent

bioRxiv preprint doi: https://doi.org/10.1101/2020.12.20.423707; this version posted March 17, 2021. The copyright holder for this preprint (which was not certified by peer review) is the author/funder, who has granted bioRxiv a license to display the preprint in perpetuity. It is made available under aCC-BY-NC-ND 4.0 International license.

experiments are shown. Parts of the results from the same experiments were previously published [28]. Chr., chromosome.

Fig S6. Chromatin association of Rpb1 in the *set2⊿rad30⊿* double mutant after DSB induction

(A-C) ChIP-qPCR analyses to determine chromatin association of Rpb1 at promoters and 3'-ends of selected genes, in G_2/M arrested cells after DSB induction. The same genes as in Fig 7C-7E were analyzed. Error bars indicate the mean ± STDEV of at least two independent experiments. n, low-binding control (n2 in Fig 1B).

Fig S7. A summary of the main results and a proposed model

In G_2/M arrested WT cells, genes belonging to the positive transcription regulation and chromatin assembly pathways are enriched compared to *rad30Δ* cells. Reduced chromatin assembly in *rad30Δ* cells results in less dynamic chromatin, indicated by additional nucleosomes. Deregulated transcription and sensitivity to elongation inhibitors in *rad30Δ* cells are indicated by thin arrows over the TSS and ORF. Histone exchange between H3 and H3K56Ac at promoter regions is reduced in the *hir1Δ* mutant, while histone exchange of H2A for H2A.Z at the +1 nucleosome is prevented in the *htz1Δ* mutant, hampering transcriptional regulation. Both mutants were deficient in damage-induced cohesion. In contrast, deletion of *SET2* compensated for reduced transcriptional capacity of the *rad30Δ* mutant, and suppressed the lack of damage-induced cohesion in *rad30Δ* cells. Taken together, histone exchange during transcription is proposed to facilitate formation of damage-induced cohesion. This

bioRxiv preprint doi: https://doi.org/10.1101/2020.12.20.423707; this version posted March 17, 2021. The copyright holder for this preprint (which was not certified by peer review) is the author/funder, who has granted bioRxiv a license to display the preprint in perpetuity. It is made available under aCC-BY-NC-ND 4.0 International license.

process is perturbed in *rad30Δ* cells, which functionally associates with transcription, thereby negatively affecting generation of damage-induced cohesion. Cells with a single green dot indicates established damage-induced cohesion while cells with two dots indicates lack of damage-induced cohesion. ORF, open reading frame.

bioRxiv preprint doi: https://doi.org/10.1101/2020.12.20.423707; this version posted March 17, 2021. The copyright holder for this preprint (which was not certified by peer review) is the author/funder, who has granted bioRxiv a license to display the preprint in perpetuity. It is made available under aCC-BY-NC-ND 4.0 International license.

S1 Table. Strains used in this study

Strain (LS)	Genotype
50	*MATa ade3::GALHO ade2-1 trp1-1 can1-100 leu2-3,112 his3-11,15 ura3-1 GAL psi+ RAD5*
421	*MATα rad30::KAN smc1-259 ade3::GALHO leu2-3,112::PGAL-SMC1-MYC-LEU2 his3-11,15::HIS3-tetR-GFP ura3-1::tetOx112-URA3 ade2-1 trp1-1 can1-100 GAL psi+ RAD5*
468	*MATα rad30(S14A)::NAT smc1-259 ade3::GALHO leu2-3,112::PGAL-SMC1-MYC-LEU2 his3-11,15::HIS3-tetR-GFP ura3-1::tetOx112-URA3 ade2-1 trp1-1 can1-100 GAL psi+ RAD5*
514	*MATa rad30::KAN ade3::GALHO ade2-1 trp1-1 can1-100 leu2-3,112 his3-11,15 ura3-1 GAL psi+ RAD5*
655	*MATa smc1-259 ade3::GALHO leu2-3,112::PGAL-SMC1-MYC-LEU2 his3-11,15::HIS3-tetR-GFP ura3-1::tetOx112-URA3 ade2-1 trp1-1 can1-100 GAL psi+ RAD5*
656/1098	MAT*α smc1-259 ade3::GALHO leu2-3,112::PGAL-SMC1-MYC-LEU2 his3-11,15::HIS3-tetR-GFP ura3-1::tetOx112-URA3 ade2-1 trp1-1 can1-100 GAL psi+ RAD5*
657	*MATa smc1-259 leu2-3,112::PGAL-SMC1-MYC-LEU2 his3-11,15::HIS3-tetR-GFP ura3-1::tetOx112-URA3 ade2-1 trp1-1 can1-100 GAL psi+ RAD5*
666	*MATa smc1-259 leu2-3,112::PGAL-SMC1-MYC-LEU2 trp1-1::PMET3-CDC20-TRP1 his3-11,15::HIS3-tetR-GFP ura3-1::tetOx112-URA3 ade2-1 can1-100 GAL psi+ RAD5*
699	*MATa htz1::HPH smc1-259 leu2-3,112::PGAL-SMC1-MYC-LEU2 trp1-1::PMET3-CDC20-TRP1 his3-11,15::HIS3-tetR-GFP ura3-1::tetOx112-URA3 ade2-1 can1-100 GAL psi+ RAD5*
847	*MATa trp1-1::PGAL-CDC20-TRP1(K. lactis) his3-11,15::HIS3-tetR-GFP ura3-1::tetOx112-URA3 ade2-1 can1-100 leu2-3,112 GAL psi+ RAD5*
848	*MATa htz1::HPH trp1-1::PGAL-CDC20-TRP1(K. lactis) his3-11,15::HIS3-tetR-GFP ura3-1::tetOx112-URA3 ade2-1 can1-100 leu2-3,112 GAL psi+ RAD5*
910	*MATa hir1::NAT smc1-259 ade3::GALHO leu2-3,112::PGAL-SMC1-MYC-LEU2 his3-11,15::HIS3-tetR-GFP ura3-1::tetOx112-URA3 ade2-1 trp1-1 can1-100 GAL psi+ RAD5*
914	*MATα hir1::NAT rad30::KAN smc1-259 ade3::GALHO leu2-3,112::PGAL-SMC1-MYC-LEU2 his3-11,15::HIS3-tetR-GFP ura3-1::tetOx112-URA3 ade2-1 trp1-1 can1-100 GAL psi+ RAD5*
928	*MATa rad61::KAN trp1-1::PGAL-CDC20-TRP1(K. lactis) his3-11,15::HIS3-tetR-GFP ura3-1::tetOx112-URA3 ade2-1 can1-100 leu2-3,112 GAL psi+ RAD5*
963	*MATa hir1::HPH smc1-259 leu2-3,112::PGAL-SMC1-MYC-LEU2 his3-11,15::HIS3-tetR-GFP ura3-1::tetOx112-URA3 ade2-1 trp1-1 can1-100 GAL psi+ RAD5*
1002	*MATα rad30::KAN smc1-259 leu2-3,112::PGAL-SMC1-MYC-LEU2 his3-11,15::HIS3-tetR-GFP ura3-1::tetOx112-URA3 ade2-1 trp1-1 can1-100 GAL psi+ RAD5*
1054	*MATa hhf1-hht1::HPH smc1-259 ade3::GALHO leu2-3,112::PGAL-SMC1-MYC-LEU2 his3-11,15::HIS3-tetR-GFP ura3-1::tetOx112-URA3 ade2-1 trp1-1 can1-100 GAL psi+ RAD5*
1055	*MATa hht2-hhf2::HPH smc1-259 ade3::GALHO leu2-3,112::PGAL-SMC1-MYC-LEU2 his3-11,15::HIS3-tetR-GFP ura3-1::tetOx112-URA3 ade2-1 trp1-1*

bioRxiv preprint doi: https://doi.org/10.1101/2020.12.20.423707; this version posted March 17, 2021. The copyright holder for this preprint (which was not certified by peer review) is the author/funder, who has granted bioRxiv a license to display the preprint in perpetuity. It is made available under aCC-BY-NC-ND 4.0 International license.

	can1-100 GAL psi+ RAD5
1056	*MATα hhf1-hht1::HPH rad30::KAN smc1-259 ade3::GALHO leu2-3,112::PGAL-SMC1-MYC-LEU2 his3-11,15::HIS3-tetR-GFP ura3-1::tetOx112-URA3 ade2-1 trp1-1 can1-100 GAL psi+ RAD5*
1057	*MATα hht2-hhf2::HPH rad30::KAN smc1-259 ade3::GALHO leu2-3,112::PGAL-SMC1-MYC-LEU2 his3-11,15::HIS3-tetR-GFP ura3-1::tetOx112-URA3 ade2-1 trp1-1 can1-100 GAL psi+ RAD5*
1090	*MATa set2::HPH smc1-259 ade3::GALHO leu2-3,112::PGAL-SMC1-MYC-LEU2 his3-11,15::HIS3-tetR-GFP ura3-1::tetOx112-URA3 ade2-1 trp1-1 can1-100 GAL psi+ RAD5*
1094	*MATa set2::HPH rad30::KAN smc1-259 ade3::GALHO leu2-3,112::PGAL-SMC1-MYC-LEU2 his3-11,15::HIS3-tetR-GFP ura3-1::tetOx112-URA3 ade2-1 trp1-1 can1-100 GAL psi+ RAD5*
1101	*MATa smc1-259 rad30::KAN ade3::GALHO leu2-3,112::PGAL-SMC1-MYC-LEU2 his3-11,15::HIS3-tetR-GFP ura3-1::tetOx112-URA3 ade2-1 trp1-1 can1-100 GAL psi+ RAD5*

bioRxiv preprint doi: https://doi.org/10.1101/2020.12.20.423707; this version posted March 17, 2021. The copyright holder for this preprint (which was not certified by peer review) is the author/funder, who has granted bioRxiv a license to display the preprint in perpetuity. It is made available under aCC-BY-NC-ND 4.0 International license.

S2 Table. Information on primary antibodies used

Antibody	Company	Catalog #
anti-Rpb1 (8WG16)	Santa Cruz Biotechnology	sc-56767
anti-Cdc11 (y-415)	Santa Cruz Biotechnology	sc-7170
anti-Rad53	Abcam	ab104232
anti-c-myc	Roche	11667203001
anti-Htz1	Active Motif	39647
anti-Histone H2A (phospho S129)	Abcam	ab15083

S3 Table. Primers used in ChIP-qPCR

Name	Sequence
ECM29 pro F	TACCAGTTTAGCCGCCAG
ECM29 pro R	CGCAATTCTGCCTTCTCC
ECM29 mid F	ATCGCAGACTCGACTCAC
ECM29 mid R	GTCACTTGGCAGACCAAC
ECM29 end F	ACACATGGAGAACGCAAC
ECM29 end R	CTTCTGAATGATCAGGCCAC
RIM4 pro F	CTCTCTTCCTTTCTCTCTCCC
RIM4 pro R	GAGTCGGCCTTTAGACCATTAG
RIM4 mid F	TGGATCATCGAATGGGCAC
RIM4 mid R	CCTCTGAATCACTACCATGCAC
RIM4 end F	TTATCCCATGTCACCACCTCC
RIM4 end R	GGTACTGCCATGATTAGCAGC
MSC1 pro F	GAGAGGGAGGAAACAAGGAG
MSC1 pro R	CGGAAACCGCATTAACCAAC
MSC1 mid F	CAGAAAAGGCAGAACAGCAG
MSC1 mid R	ACCTTGTGGCTCTCCAAC
MSC1 end F	GGTTGTTCGGCACTGTTAAG
MSC1 end R	GTACATTACGTTGACACCCC
NPL4 pro F	GCCCTCGTAACATACAGAAC
NPL4 pro R	GGTCCAGATTACCCACCAAC
NPL4 mid F	GATATACGAGCCCCCTCAG
NPL4 mid R	CAAAAAACAGACCCATCCCC
NPL4 end F	GCAGATACTCTCTCCAGACG
NPL4 end R	TCTCTCCTAGCCGCTTTC
lowbinding *TAX4* up F (n1)	CCGAAACTGCAAATCCTCC
lowbinding *TAX4* up R (n1)	TTCATCGCTCCTTTCCCC
lowbinding *ADH3* up F (n2)	CACATCCCTTTGAAACGCAC
lowbinding *ADH3* up R (n2)	TACCCTCGACAAATGCCC
31W *SPF1* pro F	GCTTCTTGTCACGCCATAC
31W *SPF1* pro R	CCCTAACAATAGGACTGCTCAC
31W *SPF1* end F	ACCTGAGCTAAACGAAGCC
31W *SPF1* end R	GCAATCTTGACCTGTTGCAC
037C *RAD23* pro F	GCTAGGCAAGAAATAGCGAC

bioRxiv preprint doi: https://doi.org/10.1101/2020.12.20.423707; this version posted March 17, 2021. The copyright holder for this preprint (which was not certified by peer review) is the author/funder, who has granted bioRxiv a license to display the preprint in perpetuity. It is made available under aCC-BY-NC-ND 4.0 International license.

037C *RAD23* pro R	TCTGCGAACGGCCTTATC
037C *RAD23* end F	GGACAAGGTGAAGGTGAAGG
037C *RAD23* end R	CGGCATGATCGCTGAATAG
039C *CYC7* pro F	GCAAGGGGCAAAGACAAAG
039C *CYC7* pro R	GTATGACACTGCTGACACC
039C *CYC7* end F	GTACCAAGATGGCGTTTGC
039C *CYC7* end R	TCTCCTCCGACGACATAGC
056W *HAT2* pro F	CTTCTGCCTCTCTTATCTCTCC
056W *HAT2* pro R	CGTGTCTCGCTAACAAAGTC
056W *HAT2* end F	GAACAAACACCTGATGACGC
056W *HAT2* end R	CGCCTTTTCGCCAAAGAAAC
060C *PRB1* pro F	CAAACACACCCGCGATAAAG
060C *PRB1* pro R	GGATGACCAAAGCAGCAG
060C *PRB1* end F	ACAACGGTGGTGGTCAAG
060C *PRB1* end R	GGACAAACGATAGTGAAGAGGG
Htz1 LBD2 F (n)	TGAGCCAGCCAACTCAGAC
Htz1 LBD2 R (n)	AAAAACTACGCCTCCACCC

Fig 1

A

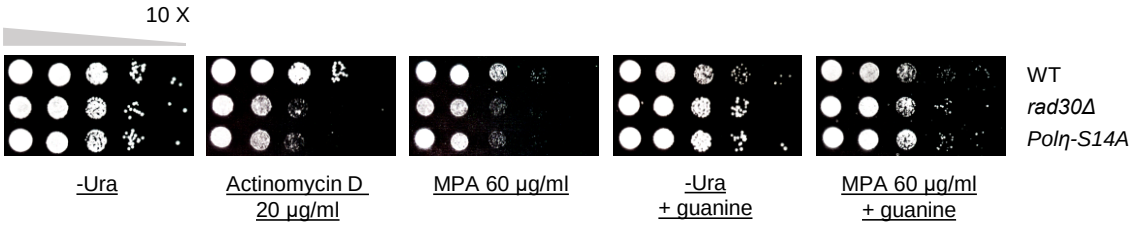

B

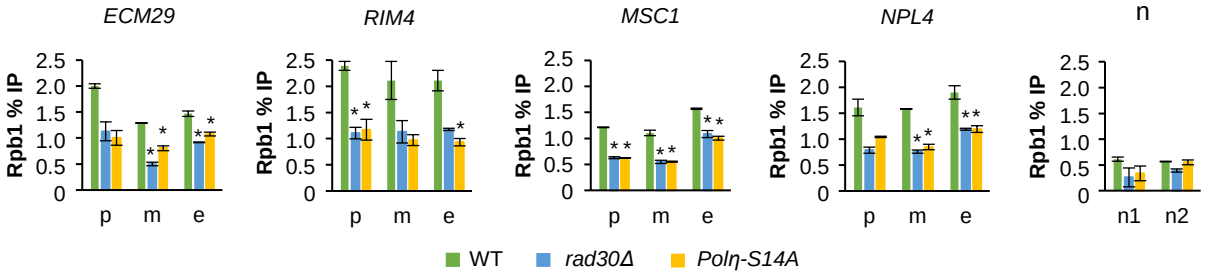

C G_2/M - P_{GAL}-*HO*

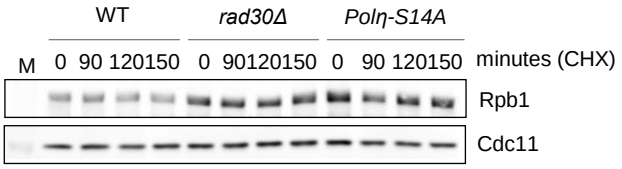

D G_2/M + P_{GAL}-*HO*

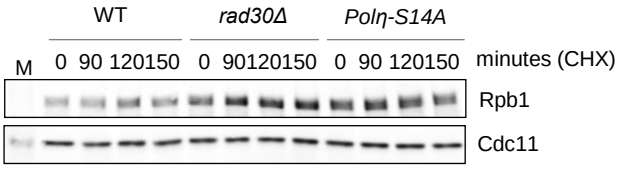

Fig 2

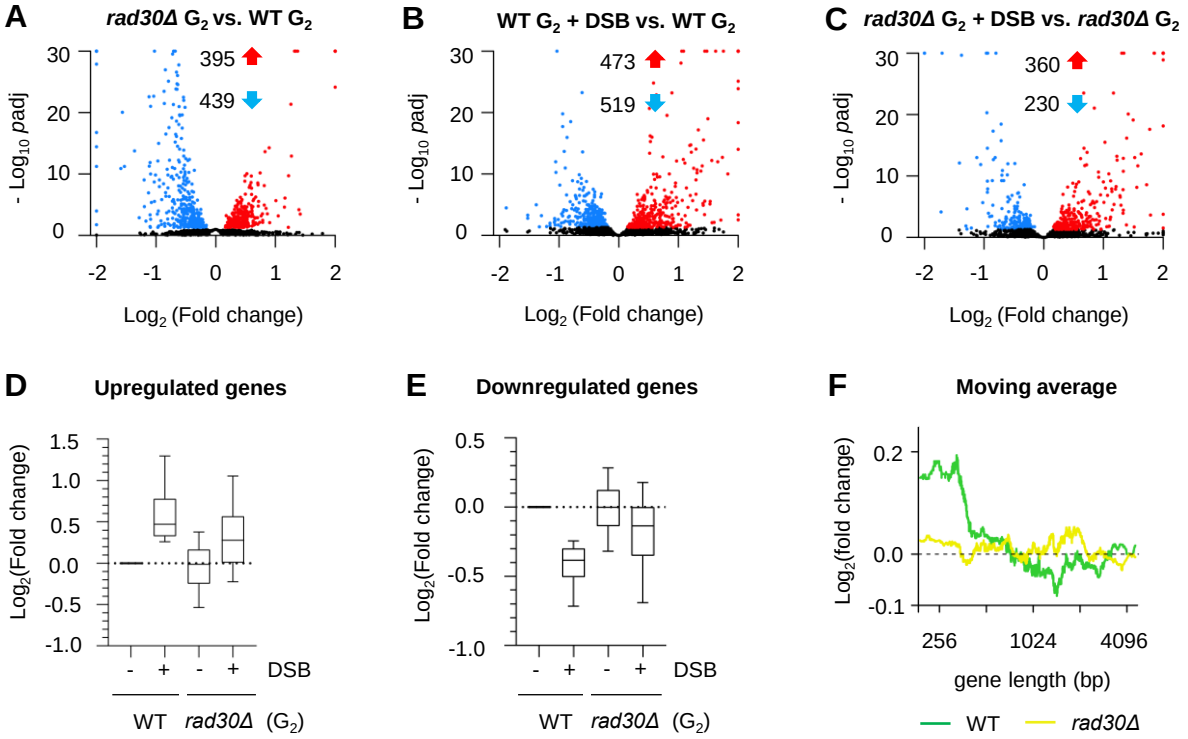
A
rad30Δ G2 vs. WT G2
395
439
- Log10 padj
Log2 (Fold change)
B
WT G2 + DSB vs. WT G2
473
519
- Log10 padj
Log2 (Fold change)
C
rad30Δ G2 + DSB vs. rad30Δ G2
360
230
- Log10 padj
Log2 (Fold change)
D
Upregulated genes
Log2(Fold change)
DSB
WT
rad30Δ
(G2)
E
Downregulated genes
Log2(Fold change)
DSB
WT
rad30Δ
(G2)
F
Moving average
Log2(fold change)
gene length (bp)
WT
rad30Δ

Fig 3

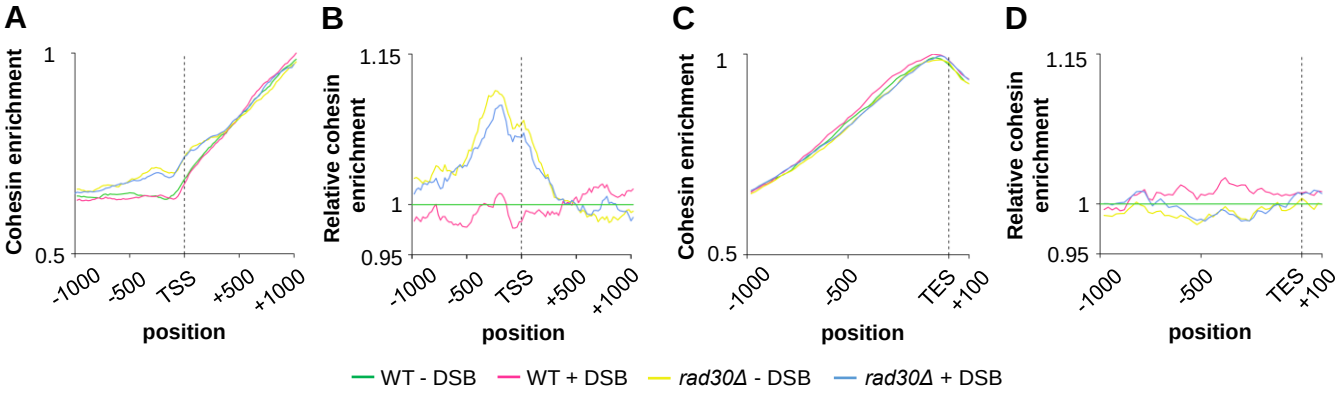
A
Cohesin enrichment
1
0.5
-1000
-500
TSS
+500
+1000
position
B
Relative cohesin enrichment
1.15
1
0.95
-1000
-500
TSS
+500
+1000
position
C
Cohesin enrichment
1
0.5
-1000
-500
TES
+100
position
D
Relative cohesin enrichment
1.15
1
0.95
-1000
-500
TES
+100
position
WT - DSB
WT + DSB
rad30Δ - DSB
rad30Δ + DSB

Fig 4

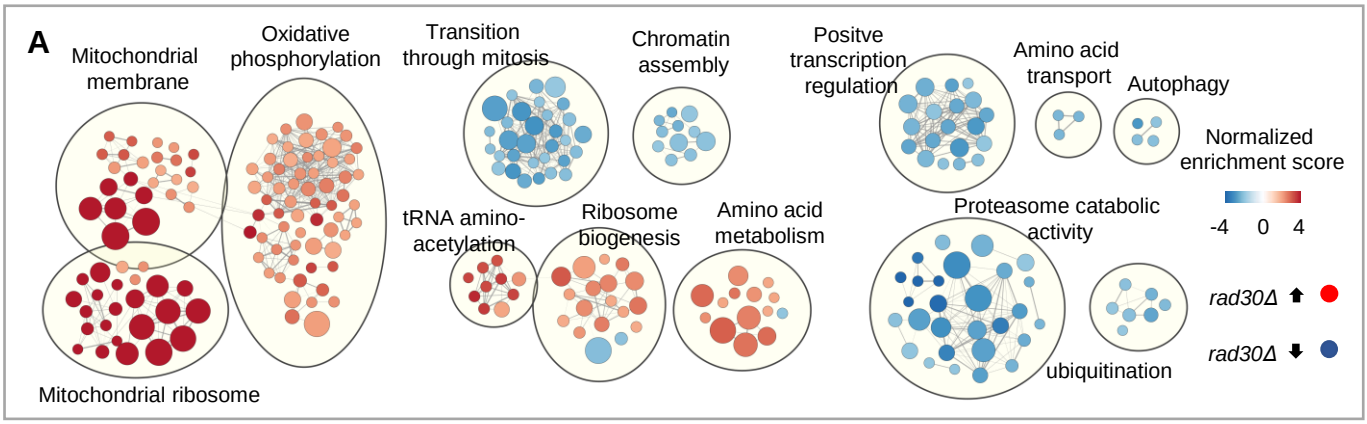
A
Mitochondrial membrane
Oxidative phosphorylation
Transition through mitosis
Chromatin assembly
Positve transcription regulation
Amino acid transport
Autophagy
Normalized enrichment score
-4 0 4
tRNA amino-acetylation
Ribosome biogenesis
Amino acid metabolism
Proteasome catabolic activity
rad30Δ
rad30Δ
ubiquitination
Mitochondrial ribosome

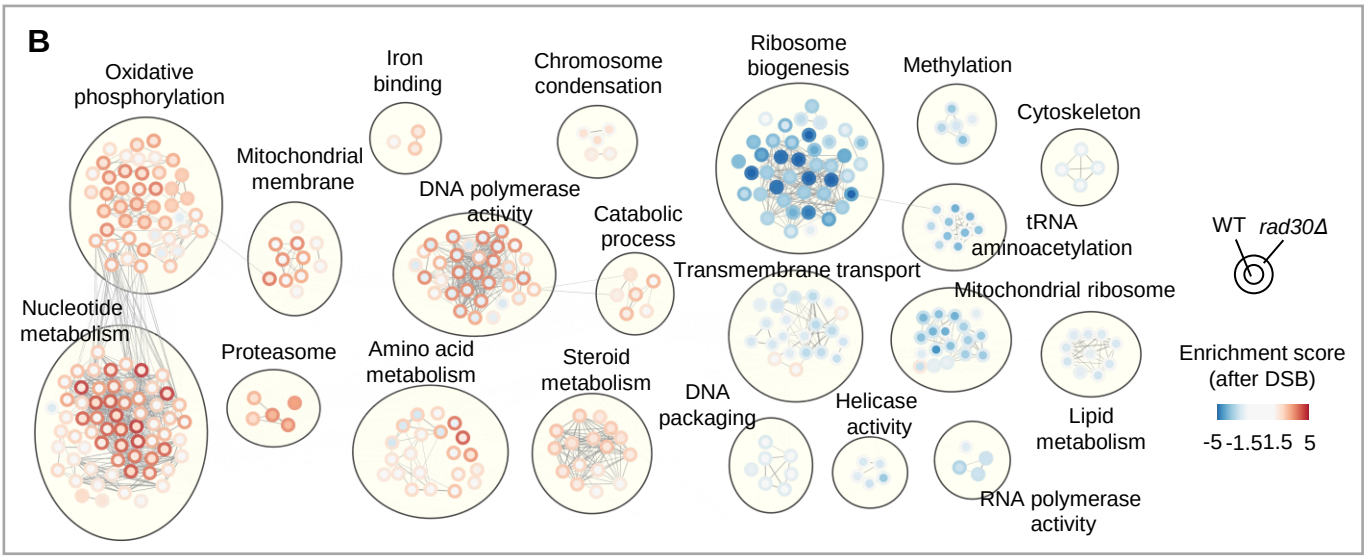
B
Oxidative phosphorylation
Iron binding
Chromosome condensation
Ribosome biogenesis
Methylation
Cytoskeleton
Mitochondrial membrane
DNA polymerase activity
Catabolic process
tRNA aminoacetylation
WT
rad30Δ
Transmembrane transport
Mitochondrial ribosome
Nucleotide metabolism
Proteasome
Amino acid metabolism
Steroid metabolism
DNA packaging
Helicase activity
Lipid metabolism
Enrichment score (after DSB)
-5 -1.5 1.5 5
RNA polymerase activity

Fig 5

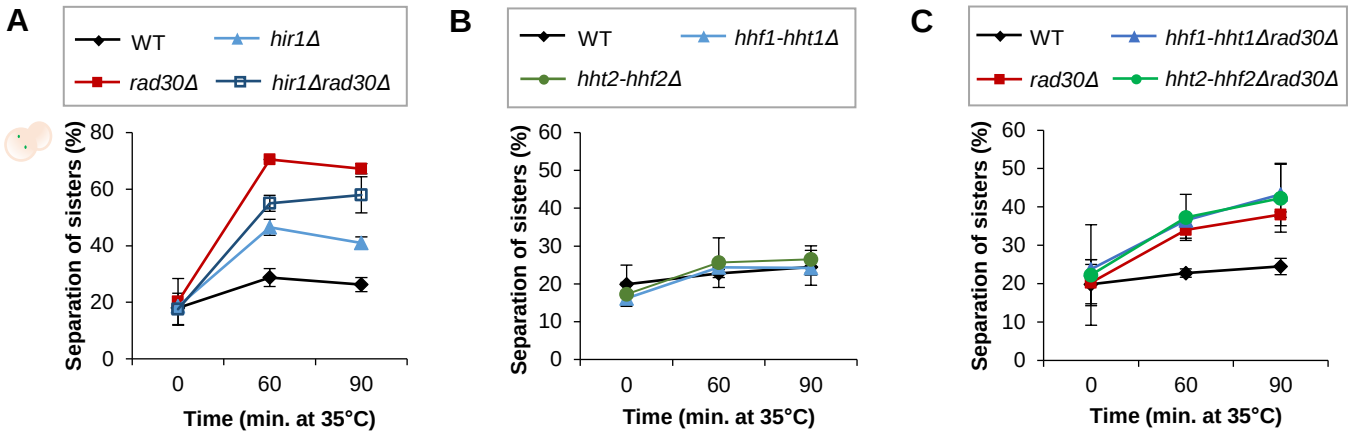
A
WT
hir1Δ
rad30Δ
hir1Δrad30Δ
Separation of sisters (%)
80
60
40
20
0
0
60
90
Time (min. at 35°C)
B
WT
hhf1-hht1Δ
hht2-hhf2Δ
Separation of sisters (%)
60
50
40
30
20
10
0
0
60
90
Time (min. at 35°C)
C
WT
hhf1-hht1Δrad30Δ
rad30Δ
hht2-hhf2Δrad30Δ
Separation of sisters (%)
60
50
40
30
20
10
0
0
60
90
Time (min. at 35°C)

Fig 6

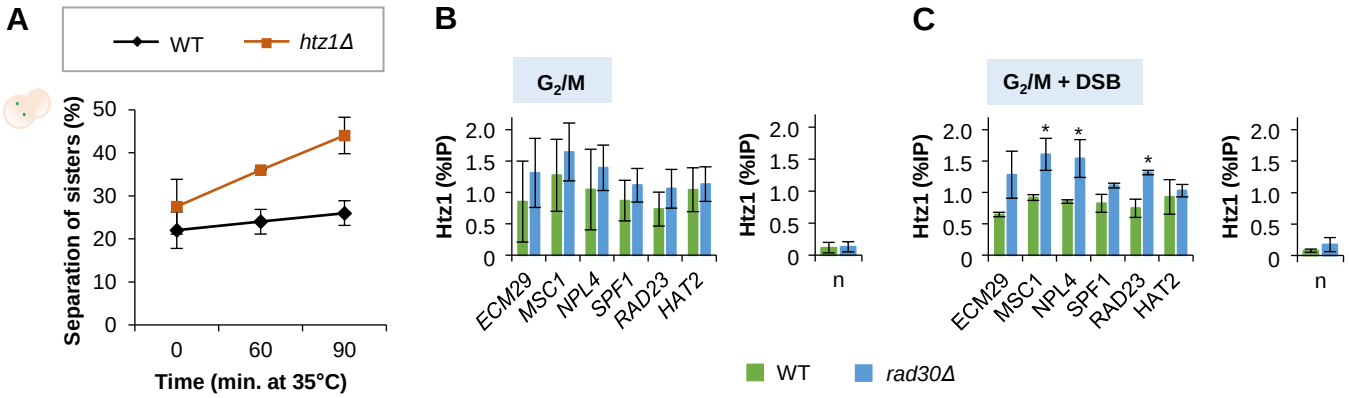
A
WT
htz1Δ
Separation of sisters (%)
50
40
30
20
10
0
0
60
90
Time (min. at 35°C)
B
G2/M
Htz1 (%IP)
2.0
1.5
1.0
0.5
0
ECM29
MSC1
NPL4
SPF1
RAD23
HAT2
n
C
G2/M + DSB
*
*
*
WT
rad30Δ

Fig 7

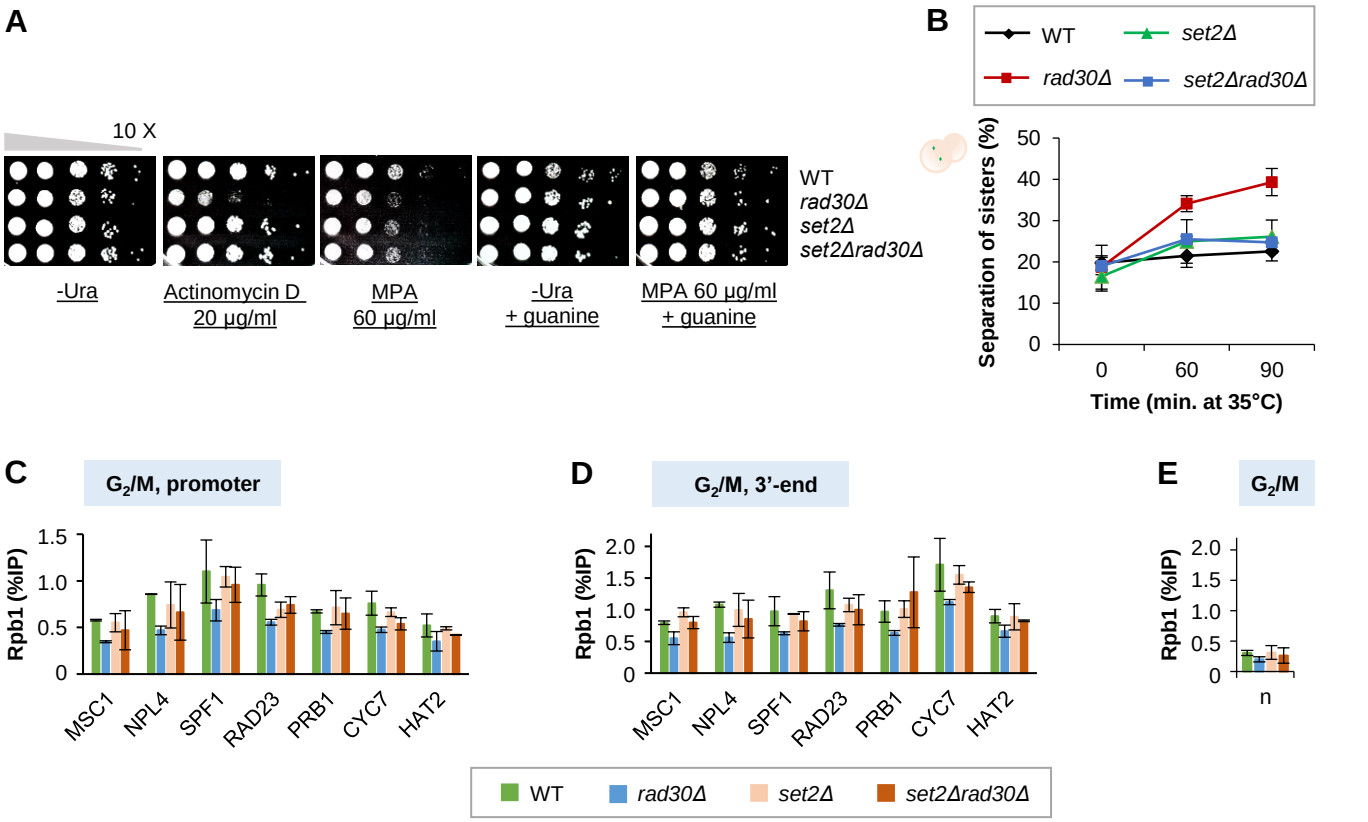
A
10 X
WT
rad30Δ
set2Δ
set2Δrad30Δ
-Ura
Actinomycin D 20 µg/ml
MPA 60 µg/ml
-Ura + guanine
MPA 60 µg/ml + guanine
B
WT
set2Δ
rad30Δ
set2Δrad30Δ
Separation of sisters (%)
Time (min. at 35°C)
C
G2/M, promoter
Rpb1 (%IP)
MSC1
NPL4
SPF1
RAD23
PRB1
CYC7
HAT2
D
G2/M, 3'-end
E
G2/M
n
WT
rad30Δ
set2Δ
set2Δrad30Δ

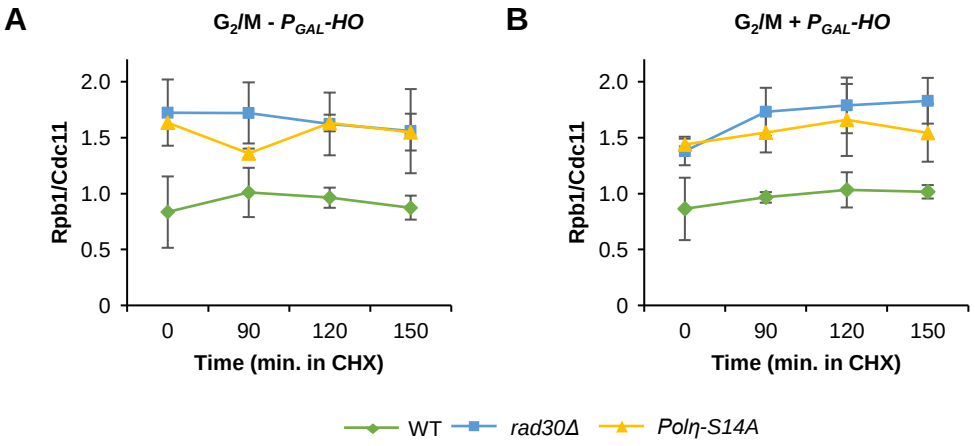
A
G2/M - PGAL-HO
B
G2/M + PGAL-HO
Rpb1/Cdc11
2.0
1.5
1.0
0.5
0
0
90
120
150
Time (min. in CHX)
WT
rad30Δ
Polη-S14A

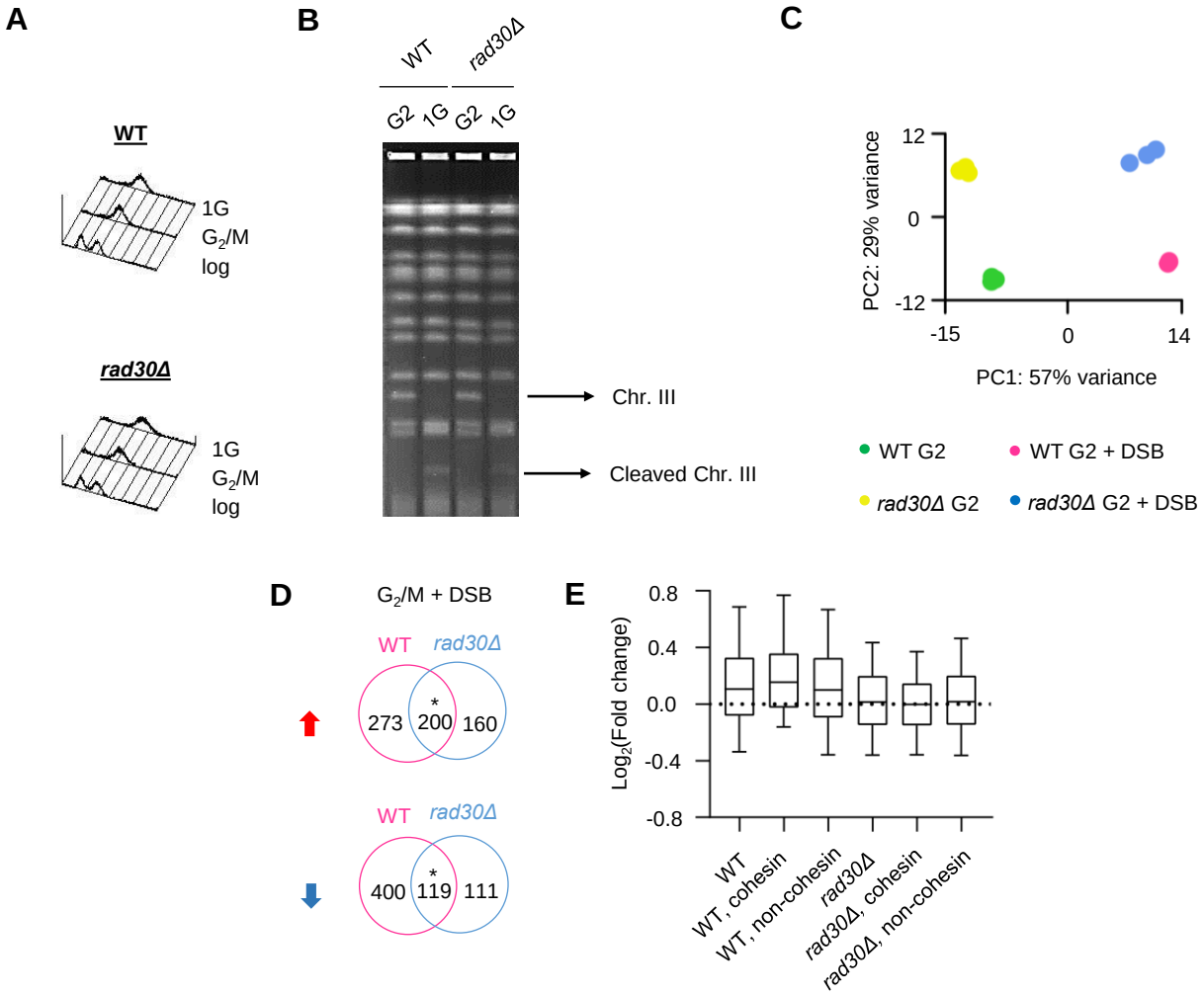
A
WT
1G
G2/M
log
rad30Δ
1G
G2/M
log
B
WT
rad30Δ
G2
1G
G2
1G
Chr. III
Cleaved Chr. III
C
PC2: 29% variance
12
0
-12
-15
0
14
PC1: 57% variance
WT G2
WT G2 + DSB
rad30Δ G2
rad30Δ G2 + DSB
D
G2/M + DSB
WT
rad30Δ
273
200
160
WT
rad30Δ
400
119
111
E
Log2(Fold change)
0.8
0.4
0.0
-0.4
-0.8
WT
WT, cohesin
WT, non-cohesin
rad30Δ
rad30Δ, cohesin
rad30Δ, non-cohesin

S3 Fig

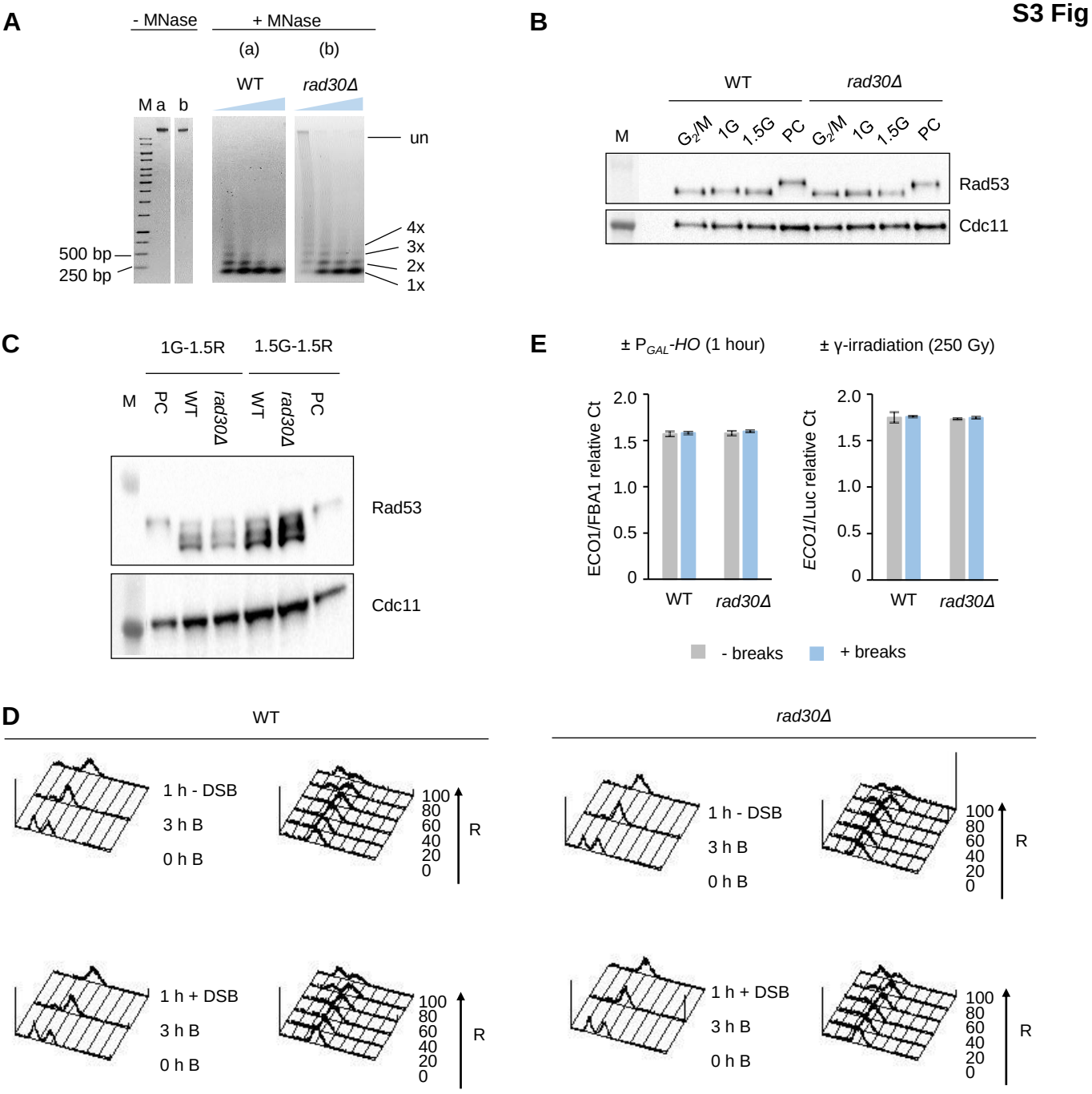
A
- MNase
+ MNase
(a)
(b)
WT
rad30Δ
M a b
un
4x
3x
2x
1x
500 bp
250 bp
B
WT
rad30Δ
M
G2/M
1G
1.5G
PC
G2/M
1G
1.5G
PC
Rad53
Cdc11
C
1G-1.5R
1.5G-1.5R
M
PC
WT
rad30Δ
WT
rad30Δ
PC
Rad53
Cdc11
E
± PGAL-HO (1 hour)
± γ-irradiation (250 Gy)
ECO1/FBA1 relative Ct
ECO1/Luc relative Ct
2.0
1.5
1.0
0.5
0
WT
rad30Δ
- breaks
+ breaks
D
WT
rad30Δ
1 h - DSB
3 h B
0 h B
1 h + DSB
3 h B
0 h B
100
80
60
40
20
0
R

S4 Fig

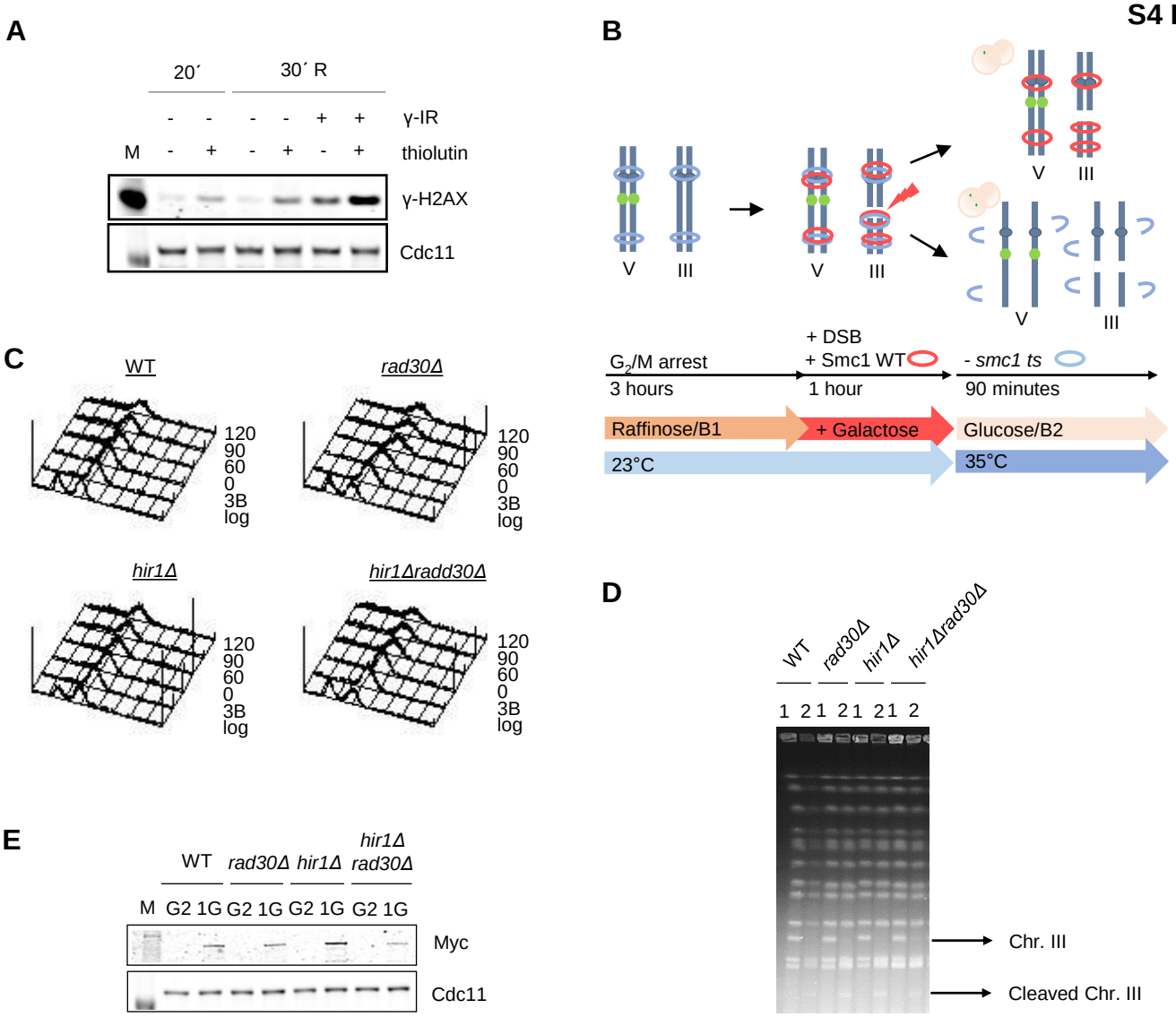
A
20´
30´ R
γ-IR
M
thiolutin
γ-H2AX
Cdc11
B
V
III
+ DSB
+ Smc1 WT
- smc1 ts
G2/M arrest
3 hours
1 hour
90 minutes
Raffinose/B1
+ Galactose
Glucose/B2
23°C
35°C
C
WT
rad30Δ
hir1Δ
hir1Δrad30Δ
120
90
60
0
3B
log
D
WT
rad30Δ
hir1Δ
hir1Δrad30Δ
1 2 1 2 1 2 1 2
Chr. III
Cleaved Chr. III
E
WT
rad30Δ
hir1Δ
hir1Δ rad30Δ
M G2 1G G2 1G G2 1G G2 1G
Myc
Cdc11

S5 Fig

A

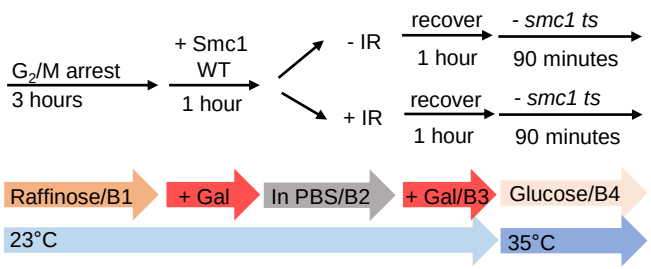
G2/M arrest
3 hours
+ Smc1
WT
1 hour
- IR
+ IR
recover
1 hour
- smc1 ts
90 minutes
Raffinose/B1
+ Gal
In PBS/B2
+ Gal/B3
Glucose/B4
23°C
35°C

B

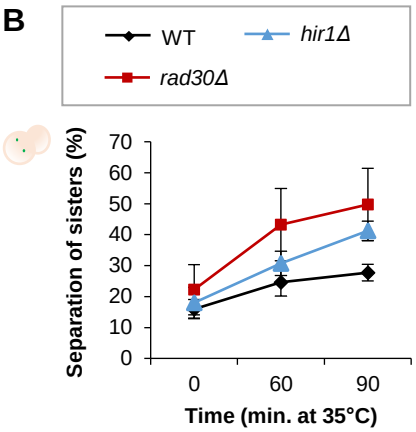
WT
hir1Δ
rad30Δ
Separation of sisters (%)
70
60
50
40
30
20
10
0
0
60
90
Time (min. at 35°C)

C

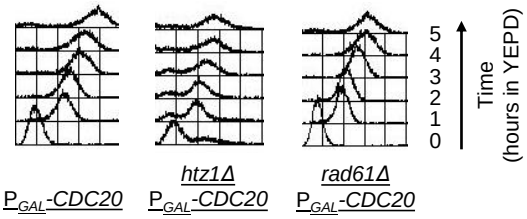
5
4
3
2
1
0
Time
(hours in YEPD)
PGAL-CDC20
htz1Δ
PGAL-CDC20
rad61Δ
PGAL-CDC20

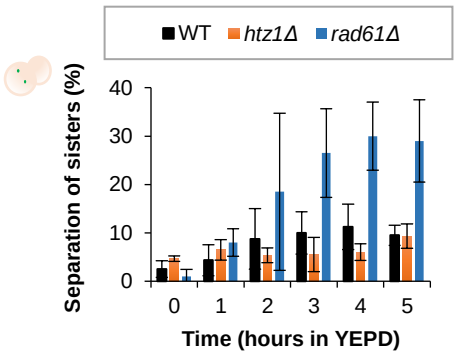
WT
htz1Δ
rad61Δ
Separation of sisters (%)
40
30
20
10
0
0
1
2
3
4
5
Time (hours in YEPD)

S6 Fig

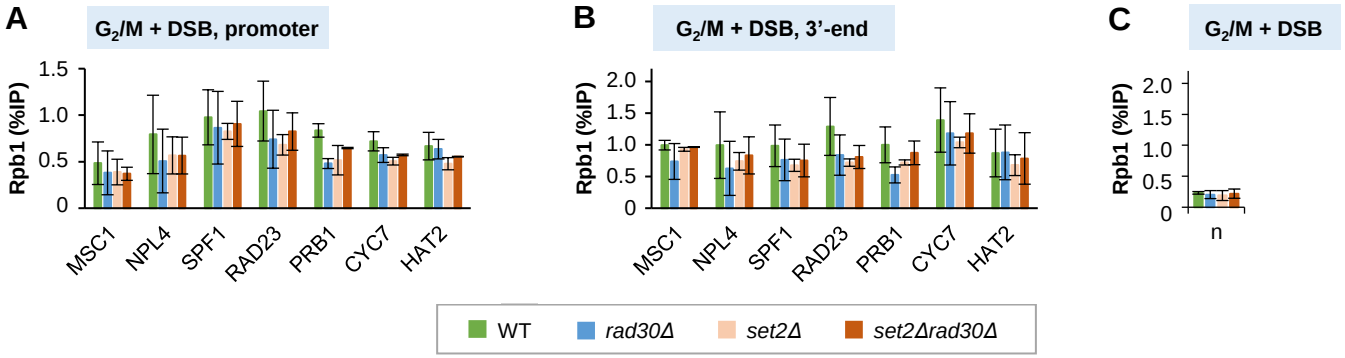
A
G2/M + DSB, promoter
Rpb1 (%IP)
1.5
1.0
0.5
0
MSC1
NPL4
SPF1
RAD23
PRB1
CYC7
HAT2
B
G2/M + DSB, 3'-end
Rpb1 (%IP)
2.0
1.5
1.0
0.5
0
MSC1
NPL4
SPF1
RAD23
PRB1
CYC7
HAT2
C
G2/M + DSB
Rpb1 (%IP)
2.0
1.5
1.0
0.5
0
n
WT
rad30Δ
set2Δ
set2Δrad30Δ

S7 Fig

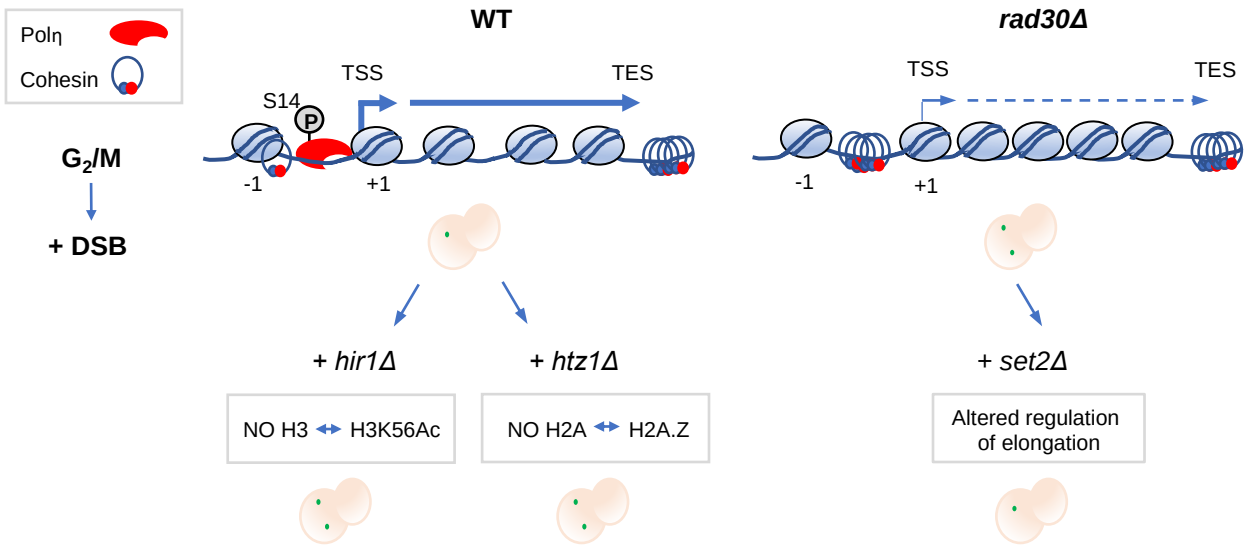
Polη
Cohesin
G2/M
+ DSB
WT
TSS
TES
S14
P
-1
+1
rad30Δ
TSS
TES
-1
+1
+ hir1Δ
+ htz1Δ
+ set2Δ
NO H3 H3K56Ac
NO H2A H2A.Z
Altered regulation of elongation